BOREAS An international journal of Quaternary research

Influence of the Laurentide Ice Sheet and relative sea-level changes on sediment dynamics in the Estuary and Gulf of St. Lawrence since the last deglaciation

MARIE CASSE, JEAN-CARLOS MONTERO-SERRANO AND GUILLAUME ST-ONGE

BOREAS

Casse, M., Montero-Serrano, J.-C. & St-Onge, G.: Influence of the Laurentide Ice Sheet and relative sea-level changes on sediment dynamics in the Estuary and Gulf of St. Lawrence since the last deglaciation. *Boreas*. 10.1111/bor.12230. ISSN 0300-9483.

Physical properties, grain size, bulk mineralogy, elemental geochemistry and magnetic parameters of three sediment piston cores recovered in the Laurentian Channel from its head to its mouth were investigated to reconstruct changes in detrital sediment provenance and transport related to climate variability since the last deglaciation. The comparison of the detrital proxies indicates the succession of two sedimentary regimes in the Estuary and Gulf of St. Lawrence (EGSL) during the Holocene, which are associated with the melting history of the Laurentide Ice Sheet (LIS) and relative sea-level changes. During the early Holocene (10–8.5 cal. ka BP), high sedimentation rates together with mineralogical, geochemical and magnetic signatures indicate that sedimentation in the EGSL was mainly controlled by meltwater discharges from the local retreat of the southeastern margin of the LIS on the Canadian Shield. At this time, sediment-laden meltwater plumes caused the accumulation of fine-grained sediments in the ice-distal zones. Since the mid-Holocene, postglacial movements of the continental crust, related to the withdrawal of the LIS (*c.* 6 cal. ka BP), have triggered significant variations in relative sea level (RSL) in the EGSL. The significant correlation between the RSL curves and the mineralogical, geochemical, magnetic and grain-size data suggest that the RSL was the dominant force acting on the sedimentary dynamics of the EGSL during the mid-to-late Holocene. Beyond 6 cal. ka BP, characteristic mineralogical, geochemical, magnetic signatures and diffuse spectral reflectance data suggest that the Canadian Maritime Provinces and western Newfoundland coast are the primary sources for detrital sediments in the Gulf of St. Lawrence, with the Canadian Shield acting as a secondary source. Conversely, in the lower St. Lawrence Estuary, detrital sediments are mainly supplied by the Canadian Shield province. Finally, our results suggest that the modern sedimentation regime in the EGSL was established during the mid-Holocene.

Marie Casse (Marie.Casse@uqar.ca; marie64casse@gmail.com), Jean-Carlos Montero-Serrano and Guillaume St-Onge, Institut des sciences de la mer de Rimouski, Canada Research Chair in Marine Geology, Université du Québec à Rimouski & GEOTOP 310 allée des Ursulines, Rimouski, QC G5L 3A1, Canada; *received 4th October 2016, accepted 23rd December 2016.*

During the early Holocene (11.5–8.2 cal. ka BP; Walker *et al.* 2012), high boreal summer insolation drove rapid retreat of the Laurentide Ice Sheet (LIS), resulting in progressive changes in the North American climate (e.g. COHMAP Members 1988; Webb *et al.* 1998; Carlson *et al.* 2007; Montero-Serrano *et al.* 2009, 2010a, 2011). During this early stage, the hydrological and sedimentary characteristics of the Estuary and Gulf of St. Lawrence (EGSL) in eastern Canada were heavily disturbed by meltwater discharges from the LIS southeastern margin and subsequent relative sea-level (RSL) variations (e.g. Dyke & Prest 1987; Shaw *et al.* 2002, 2006; St-Onge *et al.* 2011; Levac *et al.* 2015). Indeed, modifications in deglacial meltwater inputs via the St. Lawrence drainage system as the southern LIS margin retreated caused abrupt changes in sedimentation rates in the EGSL, with rates higher than ~30 m ka^{-1} during the initial deglaciation and lower rates (~40–67 cm ka^{-1}) during the early to late Holocene (e.g. St-Onge *et al.* 2003; Barletta *et al.* 2010).

In addition to impacting sedimentation rates in the EGSL, the LIS retreat also caused significant variations in relative sea level due to glacio-isostatic rebound (Dionne 1977; Clark *et al.* 1978; Shaw *et al.* 2002, 2006; Rémillard *et al.* 2016). According to Clark *et al.* (1978), the EGSL can be divided into two zones, each of them being characterized by a specific relative sea-level curve. In the EGSL, the LIS deglacial retreat exposed large areas of isostatically depressed land that were rapidly submerged (about +130 m above present level) by the transgression of the Goldthwait Sea (Zone I; Dionne 1977). In Zone I, the land rises continuously relative to sea level, and the rate of this emergence decreases through time, while Zone II is characterized by a continual submergence due to the presence of the collapsing proglacial forebulge. A domain of transition between Zones I and II is characterized by an initial emergence followed later in time by a depression of the continental crust relative to the sea surface (Clark *et al.* 1978). After ice retreat, postglacial rebound in this area caused the sea level to quickly drop below present levels (about −20 m) before they rose once more through the Holocene (e.g. Shaw *et al.* 2002). The transition from open (glacial) marine to estuarine sedimentation in the EGSL is therefore controlled by glacio-isostatic relative sea-level variations. However, the timing and magnitude of this postglacial isostatic

DOI 10.1111/bor.12230

rebound in the EGSL, and therefore of RSL, vary spatially depending on both the ice thickness and the location of a particular area relative to the ice margin (Licciardi *et al.* 1999; Dyke & Peltier 2000; Dionne & Pfalzgraf 2001; Shaw *et al.* 2002, 2006; Rémillard *et al.* 2016). The postglacial sedimentation history in the EGSL is therefore probably a product of changes in the timing and magnitude of sediment flux, glacio-isostatic adjustment and relative sea-level variations caused by the melting and retreat of the LIS.

The high sedimentation rates (~40–67 cm ka^{-1}; Barletta *et al.* 2010) and the relatively fine-grained postglacial sediments deposited in the Laurentian Channel offer unique records for reconstructing sediment dynamics and past climate conditions at the centennial to millennial time scales. However, in spite of these exceptional sedimentary characteristics, the nature, origin and transport of detrital sediments in the EGSL as well as its variability over time have been poorly documented (e.g. D'Anglejan 1969; D'Anglejan & Smith 1973; Pinet *et al.* 2011). Moreover, mineralogical, geochemical and magnetic signatures of the terrigenous components transported by rivers of the north and south coasts towards the EGSL are specific to the drainage areas where the two main geological provinces (Greenville and Appalachian) contain different bulk mineral assemblages and geochemical signatures (e.g. Loring & Nota 1973; Jaegle 2015). These proxies may therefore help to highlight the evolution of sedimentary inputs in the EGSL since the last deglaciation.

Using a multiproxy approach (including physical properties, magnetic parameters, grain size, bulk mineralogy and elemental geochemistry) on three piston cores recovered along an east–west transect in the Laurentian Channel (from its head to its mouth), we aimed to: (i) reconstruct changes in sediment provenance and transport related to climatic and oceanographic variability and (ii) provide new insights on potential relations between sea-level variations and sediment dynamics in the EGSL since the last deglaciation.

Physiographical and geological setting of the Estuary and Gulf of St. Lawrence

The EGSL is a transitional environment between the St. Lawrence River and the northwest Atlantic Ocean. Circulation in the EGSL is therefore estuarine, with a lower salinity surface layer flowing seawards and saltier intermediate and deep layers flowing landwards (Koutitonsky & Bugden 1991). Large seasonal contrasts in surface waters range from freezing conditions in winter (allowing the formation of sea ice) to temperate conditions in summer due to a very strong seasonal cycle in the overlying air temperature (e.g. Saucier *et al*. 2003; Smith *et al.* 2014).

The annual mean circulation in the EGSL is principally characterized by coastal currents that dominantly flow in an E–W direction (such as the Gaspé Current), the Anticosti Gyre and by the inflowing West Newfoundland Current that flows northward along the west coast of Newfoundland (Fig. 1A). These currents are characterized by a mean speed in the order of ~1 cm s^{-1} (Tang & Bennett 1981). In the EGSL, one of the most striking features of near surface circulation is the Gaspé Current, which is a buoyancy-driven coastal jet originating in the St. Lawrence Estuary (near Rimouski) and flowing seaward along the coast of the Gaspé Peninsula (Sheng 2001). This current disperses the South Shore St. Lawrence runoff into the northwestern and the southern Gulf (e.g. Loring & Nota 1973). In addition, according to circulation models for the EGSL (Galbraith *et al.* 2016), currents are the strongest in the surface mixed layer, generally 0–20 m (Fig. 1A), except during the winter months when the 20–100 m and the 100 m to bottom averages are almost as high (Galbraith *et al.* 2016). Currents are also the strongest along the slopes of the deep channels such as the Laurentian Channel (Galbraith *et al.* 2016).

The EGSL bathymetry is profoundly marked by a submarine U-shaped valley resulting from Quaternary glacial erosion and deposition – the Laurentian Channel (King & MacLean 1970; Loring & Nota 1973; Piper *et al.* 1990). This dominant topographical feature (250–500 m deep) extends from the eastern Canadian continental shelf to the mouth of the Saguenay Fjord near Tadoussac and contains a very thick (>450 m) Quaternary sedimentary succession (St-Onge *et al.* 2008; Duchesne *et al.* 2010). This thick infill is mainly attributable to high sedimentation rates (~100–400 cm ka^{-1}; Barletta *et al.* 2010) driven by the rapid hinterland retreat of the LIS during the last deglaciation and its subsequent meltwater discharges transported into the EGSL via the St. Lawrence River system (e.g. St-Onge *et al.* 2003, 2008; Mattheus *et al.* 2007). Recent seismic data from the EGSL reveal eight seismic units in the Quaternary succession (Duchesne & Bellefleur 2007; Duchesne *et al.* 2010). Units 1 and 2 have a highly variable thickness and fill most of the two major bedrock depressions that exist in the lower St. Lawrence Estuary. Unit 1, which records over 150 m of sediments (with very high sediment accumulation rates), is attributed to either deglacial sediments or pre-Wisconsinan sediments (i.e. Marine Isotopic Stages ≥5, St-Onge *et al.* 2008). Unit 2 is observed under a thick sediment sequence reaching >250 m in the lower St. Lawrence Estuary and thinning out to <5 m in the Honguedo Strait (St-Onge *et al.* 2008). The lower part of seismic Unit 2 was deposited during a phase of stabilization marked by local re-advances of the LIS margin in the Goldthwait Sea that began at or before the Younger Dryas (St-Onge *et al.* 2008). Unit 3, which filled ponded-basins found on the bordering shelves of the estuary, is correlated with glaciomarine

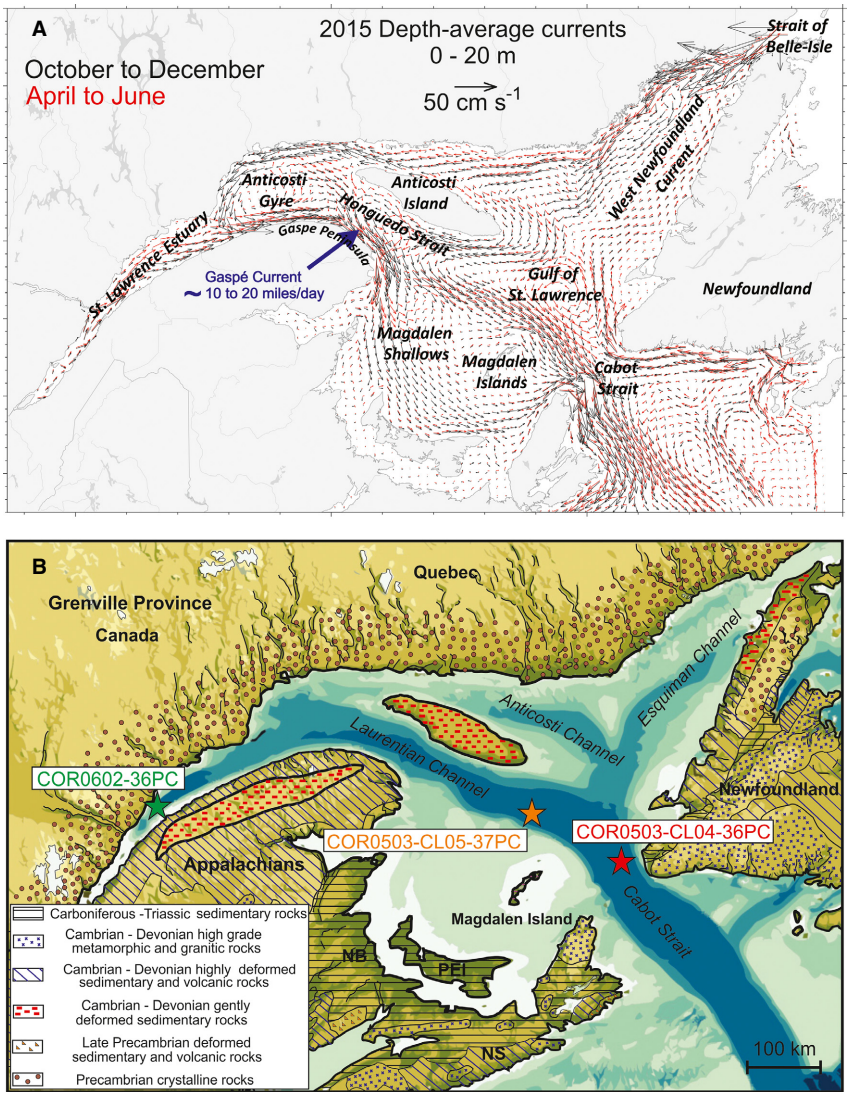

Fig. 1. A. Simplified oceanic circulation models from the Estuary and Gulf of St. Lawrence (modified from Galbraith *et al.* 2016) between October to December (black vectors) and April to June (blue vectors). B. Simplified geological map of the land adjacent to the Estuary and Gulf of St. Lawrence (modified from Loring & Nota 1973) showing the location of the three sediment piston cores studied herein.

clays (≥8.5 cal. ka BP). Units 4 and 5 were deposited in a hemipelagic setting and are correlated to postglacial sediments (≤8.5 cal. ka BP; St-Onge *et al.* 2003). Units 6, 7 and 8 were deposited by local sedimentary processes associated with submarine fans, mass wasting events and contourite deposits (Duchesne & Bellefleur 2007; St-Onge *et al.* 2008; Duchesne *et al.* 2010). Likewise, high-resolution seismic reflection data in conjunction with piston coring indicate that tills, glaciomarine sediments, and postglacial muds characterize the regional stratigraphy of the EGSL for the late Pleistocene to Holocene (e.g. Loring & Nota 1973; Josenhans & Lehman 1999; Duchesne *et al.* 2010; St-Onge *et al.* 2011). Moreover, surface sediments in the EGSL are characterized by fine-grained sediments (notably, fine silts) in the deep central parts of the Laurentian Channel and by coarser-grained sediments (gravels, sands and, to a lesser proportion, fine silts) in the slopes and adjacent shelves (Loring & Nota 1973; St-Onge *et al.* 2003; Pinet *et al.* 2011; Jaegle 2015).

Total suspended matter in the EGSL is about 60–90% detrital (e.g. D'Anglejan & Smith 1973). Detrital sedimentation in this area is influenced by seasonal changes in rain and snow precipitation on the continent, freshwater discharges, atmospheric circulation, tidal current, wave energy and by the formation of sea ice (e.g. D'Anglejan & Smith 1973; Dionne 1993; Saucier *et al.* 2003; Hargrave *et al.* 2007; Scully & Friedrichs 2007). In fact, nearshore sediment dynamics of

the EGSL are dominated by sea ice (e.g. Dionne 1993; Neumeier 2011), due to its capacity to transport sediments from clay to boulders, erode tidal marshes and tidal flats, and, thus, participate in the regional erosion budget (Drapeau 1992).

Sedimentary inputs in the EGSL derive mainly from the Grenvillian metamorphic rocks of the Canadian Shield on the North Shore as well as from the early Palaeozoic sedimentary rocks of the Appalachian domain on the South Shore, Canadian Maritime Provinces and western Newfoundland coast (Loring & Nota 1973; Jaegle 2015). These two geological provinces have drastically different mineralogical, geochemical and magnetic signatures (Fig. 1B): (i) Grenvillian metamorphic rocks are characterized by high amphibole, potassium feldspar, plagioclase feldspar and magnetite contents as well as high magnetic susceptibility, whereas (ii) Palaeozoic sedimentary rocks of the Appalachian domain are characterized by high quartz, phyllosilicates (mainly biotite and muscovite) and hematite contents, and low magnetic susceptibility (Loring & Nota 1973; Jaegle 2015). In addition, the Palaeozoic sedimentary rocks (including limestone, dolostone and calcareous shale) cropping out on Anticosti Island and the western Newfoundland coast may also contribute local detrital sediments to the Gulf of St. Lawrence (e.g. Loring & Nota 1973; Ebbestad & Tapanila 2005). Overall, an important conclusion to draw from these studies is that mineralogical, geochemical and magnetic variations recorded in the Laurentian Channel sediments may be attributed to changes in the relative contributions of various sediment sources.

Material and methods

Samples

Three sediment cores from the lower St. Lawrence Estuary (COR0602-36PC) and Gulf of St. Lawrence (COR0503-CL04-36 and COR0503-CL05-37) were collected on board the research vessel (R/V) 'Coriolis II' during two different cruises in June 2005 (COR0503) and 2006 (COR0602) (Table S1). These sediment cores were recovered along the axis of the Laurentian Channel, from its head to its mouth (Fig. 1B), using a piston corer, allowing the sampling of cores up to 7.90 m. All coring sites were targeted using high-resolution seismic profiles that indicated high sediment accumulation not influenced by mass wasting events (Barletta *et al.* 2010).

Samples for bulk mineralogical analysis were evenly sampled at 5-cm intervals (total of 456 samples). Complementarily, major and minor element concentrations were determined at 15-cm intervals, whereas sediment grain-size analyses were performed at 10-cm intervals. Before the bulk mineralogical and geochemical analysis and in order to isolate the detrital fraction from these sediment samples, organic matter and biogenic carbonate were removed with 10 mL of peroxide (30%) and 10 mL of hydrochloric acid (0.5 N), respectively. Biogenic silica was not removed as it appeared to be negligible (probably <1%, as suggested by the fact it was not detected in the bulk sediment X-ray diffraction (XRD) diffractograms). Next, sediment samples were rinsed five times with distilled water and ground with a McCrone micronizing mill with agate grinding elements to obtain a consistent grain size of <10 μm using 5 mL of ethanol and grinding times of 5–10 min to obtain a homogenous powder. The slurry was oven dried overnight at about 60 °C and then slightly homogenized with an agate mortar to prevent the possible agglomeration of finer particles during drying. Aliquots of these homogenized sediment samples were used for bulk mineralogical and geochemical analysis.

Chronostratigraphic framework

The chronostratigraphic framework of all sediment cores used in this study was published previously and derived from 17 AMS-^{14}C ages obtained on marine mollusc shell fragments (Barletta *et al.* 2010). Further support of the age model of core COR0602-36PC comes from comparison of magnetic susceptibility profiles of the lower part (562 cm) of the core with nearby core MD99-2221 (St-Onge *et al.* 2003) (Fig. S1). Characteristic peaks in both magnetic susceptibility curves have been identified in order to transfer the age model of core MD99-2221 to core COR0602-36PC below 562 cm where no radiocarbon ages are available. The R software package BACON (Blaauw & Christen 2011) was used to produce the 'best fit' linearly interpolated age models. BACON uses a Bayesian approach to estimate the best fit or weighted mean age for each depth with a 95% confidence interval. Overall, the chronostratigraphic framework of all these sediment cores suggests high sedimentation rates in the last 10 cal. ka BP (300 to 40 cm ka^{-1}; Fig. 2).

Analytical procedure

Physical properties: multisensor core logger analyses. – The physical properties were measured using a GEOTEK Multi Sensor Core Logger (MSCL) at the Institut des sciences de la mer de Rimouski (ISMER). Diffuse spectral reflectance data were acquired at 5-cm resolution immediately after splitting the core, using an X-Rite DTP22 hand-held spectrophotometer and are reported in the L*, a*, b* colour space of the International Commission on Illumination (CIE). L* is a black to white scale, a* is a green to red scale and b* is a blue to yellow scale (e.g. St-Onge *et al.* 2007; Debret *et al.* 2011). Note that a* was only used in this study because this can be a useful parameter to detect

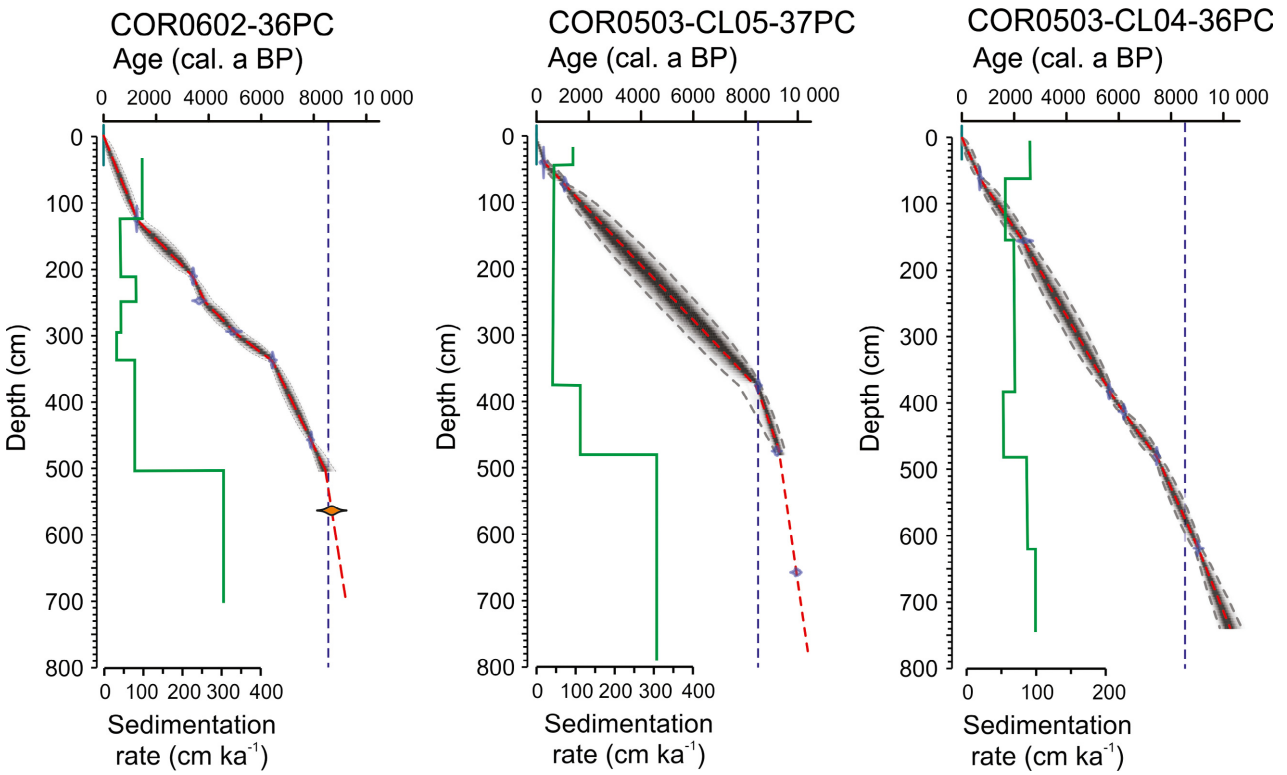

Fig. 2. Age models for cores COR0602-36PC, COR0503-CL05-37PC and COR0503-CL04-36PC. Modified from Barletta *et al.* (2010). The age–depth relationship was built with a Bayesian approach using the R-package Bacon (Blaauw & Christen 2011). The red dashed line shows the best age model and the black shading represents the chronological uncertainties (95% confidence interval). The green line shows the changes in sedimentation rates along depth. The vertical dashed line depicts the important change in the sedimentation rates observed in cores COR0602-36PC and COR0503-CL05-37PC from the St. Lawrence maritime estuary at *c.* 8.5 cal. ka BP (Barletta *et al.* 2010).

changes in the concentration of high-coercivity red minerals such as hematite (St-Onge & Lajeunesse 2007).

Grain size distribution and end-member modelling analysis. – Sediment grain-size analyses were performed on bulk sediment samples using a Beckman Coulter LS13320 laser diffraction grain-size analyser. Deflocculation of the samples was done by mixing about 0.5 g of wet sediment with Calgon electrolytic solution (sodium hexametaphosphate, 20 g L^{-1}) and subsequently shaken for at least 3 h using an in-house rotator. Grain-size distribution and statistical parameters (e.g. mean, sorting) were calculated using the moment methods from the GRADISTAT software (Blott & Pye 2001). Also, the end-member modelling algorithm (EMMA) developed by Weltje (1997) and adapted by Dietze *et al.* (2012) was applied to the grain-size data in order to extract meaningful end-member (EM) grain-size distributions and estimate their proportional contribution to the sediments. The cumulative explained variance (r^2) was calculated in order to assess the minimum number of EMs needed for a good estimate of our grain-size data (e.g. Weltje 1997; Prins & Weltje 1999; Dietze *et al.* 2012). A more detailed description of the EMMA method that we applied can be found in Dietze *et al.* (2012). Overall, grain-size distribution and end-member modelling analysis were used to investigate the sedimentary transfer regime because sediment grain-size distribution (primarily driven by sedimentary processes) reflects transport conditions (e.g. Montero-Serrano *et al.* 2009, 2010a; Dietze *et al.* 2012; Simon *et al.* 2012; Stuut *et al.* 2014).

Bulk sediment mineralogy. – The random powder samples were side-loaded into the holders and analysed by XRD using a PANalytical X'Pert Powder diffractometer. This instrument is fitted with a copper tube (Cu K-alpha = 1.54178Å) operating at 45 kV and 40 mA and a post-diffraction graphite monochromator. Samples were scanned from 5° to 65° two-theta in steps of 0.02° two-theta and a counting time of 2 s per step. For the semi-quantification of the major mineralogical components, the bulk sediment XRD scans obtained were processed in the software package X'Pert High-Score Plus (PANalytical) using the Rietveld full-pattern fitting

method (e.g. Young 1993; Grunsky *et al.* 2013). This method permits the semi-quantification of whole-sediment mineralogy with a precision of 5–10% for phyllosilicate and 5% for non-phyllosilicate minerals. The quality of the Rietveld fitting procedure was evaluated for two statistical agreement indices: R-profile and goodness-of-fit (GOF). R-profile quantifies the difference between the observed and calculated patterns, whereas the GOF is the ratio between the R-weighted profile (RWP; best fit of least squares between observed and calculated patterns) and R-expected theoretical (Rexp; best possible value for the residual). R-value profiles between 20–30% and GOFs of <3 are typically adequate in the Rietveld refinement of geological samples (e.g. Young 1993). The major mineralogical components quantified by this technique are: quartz, potassium feldspar (microcline + orthoclase), plagioclase feldspar (albite + anorthite), amphibole (hornblende), pyroxene (augite), magnetite, hematite, goethite, calcite, dolomite and phyllosilicates (biotite, muscovite, illite, chlorite and kaolinite).

Elemental geochemistry. – A total of 14 elements (Al, Si, K, Mg, Ca, Ti, Mn, Fe, P, Sr, V, Cr, Zn and Zr) were analysed by energy dispersive X-ray fluorescence (EDXRF) spectrometry using a PANalytical Epsilon 3-XL. Before EDXRF analysis, loss on ignition (LOI) was determined gravimetrically by heating the dried samples up to 950 °C for 2 h. Subsequently, samples were treated by borate fusion in an automated fusion furnace (CLAISSE® M4 Fluxer). Samples weighing ~0.6 g were mixed with ~6 g of lithium borate flux (CLAISSE, pure, 49.75% $Li_2B_4O_7$, 49.75% $LiBO_2$, 0.5% LiBr). The mixtures were melted in Pt-Au crucibles (95% Pt, 5% Au), and after fusion, the melts were cast to flat discs (diameter: 32 mm; height: 3 mm) in Pt–Au moulds. Acquired XRF spectra were processed with the standardless Omnian software package (PANalytical). The resulting data are expressed as weight percent (wt.%; Al, Si, K, Mg, Ca, Ti, Mn, Fe, P) and micrograms per gram (μg g^{-1}; V, Cr, Zn, Sr, Zr). Procedural blanks always accounted for <1% of the lowest concentration measured in the sediment samples. Analytical accuracy and precision were found to be better than 1–5% for major elements and 5–10% for the other elements, as checked by an international standard (USGS SDC-1) and analysis of replicate samples.

Magnetic remanence analyses. – The isothermal remanence magnetization (IRM) and saturated isothermal remanent magnetization (SIRM) measurements of all the sediment cores used in this study were published previously by Barletta *et al.* (2010). These measurements were acquired on u-channel samples at 1-cm intervals using a 2G Enterprises SRM-755 cryogenic magnetometer in order to identify and characterize the magnetic concentration, mineralogy and grain size. The IRM was imparted using a 2G Enterprises pulse magnetizer with a direct current field of 0.3 T, whereas the SIRM was imparted using a field of 0.95 T. We use the IRM/SIRM ratio measured at 0 mT (referred to as the pseudo S-ratio, St-Onge *et al.* 2003) to estimate the magnetic mineralogy, with values close to 1 indicating lower coercivity minerals such as magnetite, whereas lower values indicate a contribution from higher coercivity minerals such as hematite (Stoner & St-Onge 2007).

Statistical approach

The mineralogical and geochemical data are of a compositional nature, that is, they are vectors of non-negative values subjected to a constant-sum constraint (100%). This implies that relevant information is contained in the relative magnitudes, so statistical analysis must focus on the ratios between components (Aitchison 1986). In this context, principal component analysis (PCA) was performed on the mineralogical and elemental geochemical data sets with the goal of finding associations with similar relative variation patterns that may be interpreted from a palaeoenvironmental standpoint (e.g. Von Eynatten *et al.* 2003, 2016; Montero-Serrano *et al.* 2010b, 2015). For the PCA with mineralogical data, we selected four key minerals (quartz, K-feldspar, plagioclase and phyllosilicates) that represented more than 97% of the overall mineral concentration in the sediment sample. For the PCA with elemental data, we used all major and minor elements analysed as well as LOI. Prior to PCA, a log-centred (clr) transform was applied to the data set (Aitchison 1990). The clr transform is derived by dividing each variable (e.g. mineral percentage, element concentration) by the geometric mean of the composition of the individual observations and then taking the logarithm. This operation removes statistical constraints on compositional variables, such as the constant-unit sum, and allows the valid application of classical (Euclidean) statistical methods to compositional data (Aitchison 1986, 1990). PCA was conducted with R software using the package 'compositions' (Van den Boogaart & Tolosana-Delgado 2008) (Fig. 3).

All analytical data presented are available electronically in the PANGAEA database (https://doi.pangaea.de/10.1594/PANGAEA.868771).

Results

Sediment characteristics and chronostratigraphic framework

In this study, all the sediment cores present two distinct sedimentary units. According to Barletta *et al.* (2010),

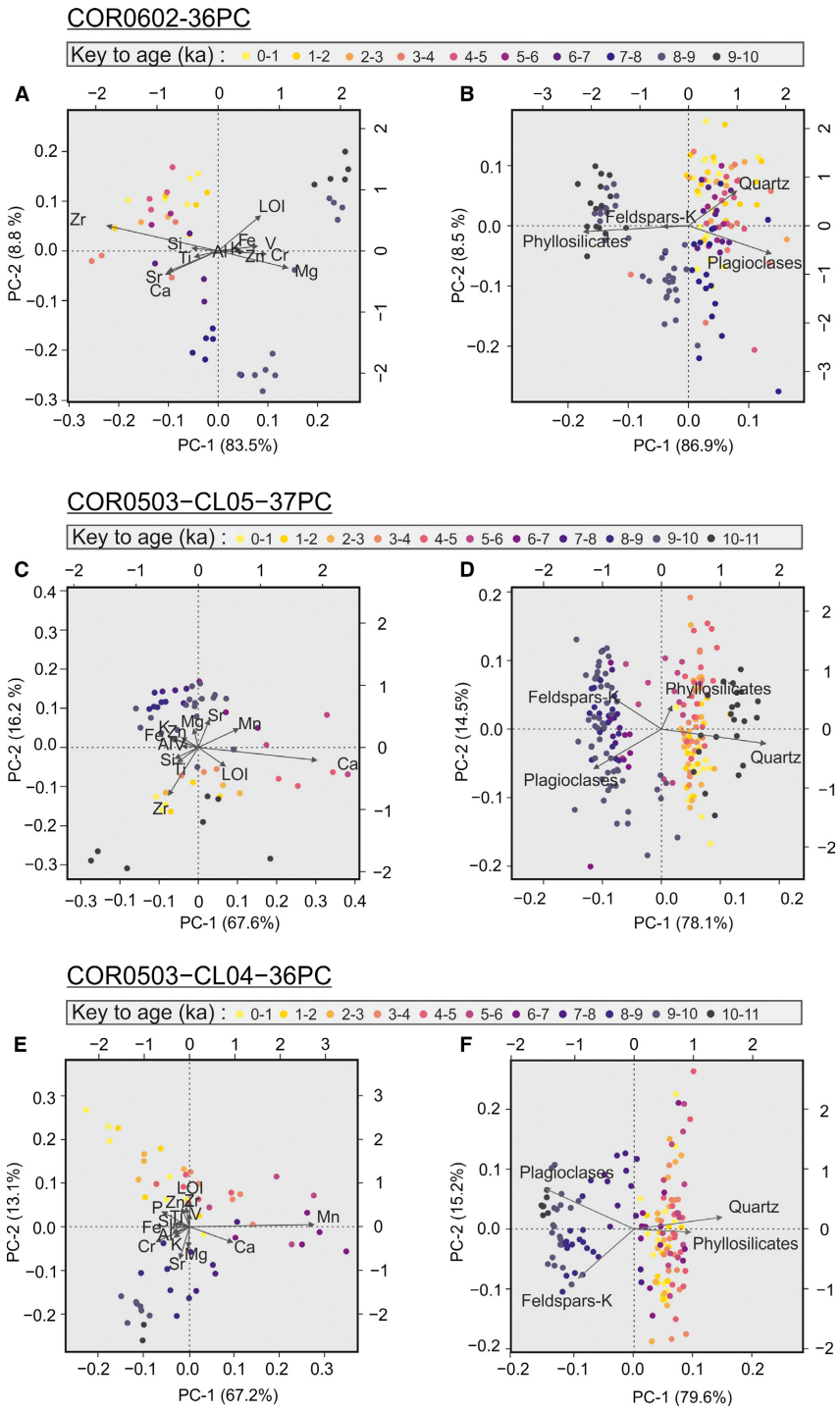

Fig. 3. Biplots of the PC-1 vs. PC-2 obtained from the log-centred transformation of the bulk mineralogical and geochemical data for cores COR0602-36PC (A, B), COR0503-CL05-37PC (C, D) and COR0503-CL04-36PC (E, F).

the upper unit is composed of dark grey, bioturbated silty clays to sandy mud, whereas the lower unit is composed of lighter grey and relatively homogeneous, slightly bioturbated clayey silts to silty clays (Fig. 4). The mean sedimentation rates of the cores COR0602-36PC and COR0503-CL05-37PC revealed an abrupt change around 8.5 cal. ka BP, with variations from ~300 to ~40 cm ka^{-1} (Fig. 2). Conversely, the core located at the most seaward location (COR0503-CL04-36PC) does not show any significant change in

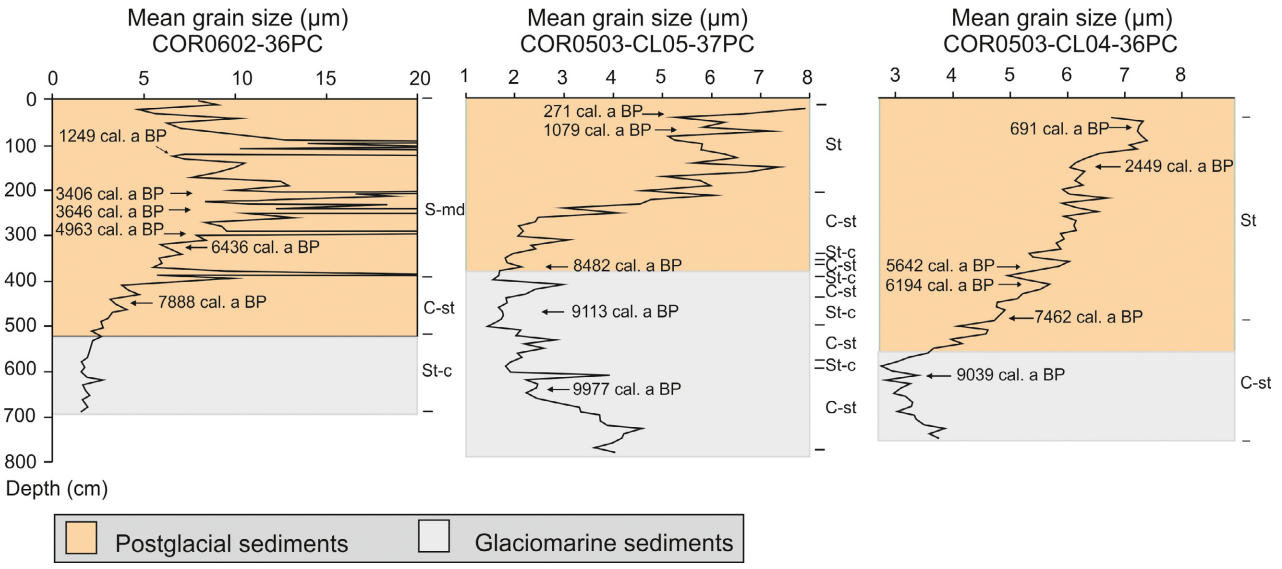

Fig. 4. Mean grain size vs. depth for cores COR0602-36PC, COR0503-CL05-37PC and COR0503-CL04-36PC. The grey and orange areas represent glaciomarine and postglacial sediments, respectively. The sediment texture is indicated to the right of each diagram. St-c = silty clays; C-st = clayey silts; St = silts; S-md = sandy muds. Modified from Barletta *et al.* (2010).

the mean sedimentation rates (~75 cm ka^{-1}) throughout the Holocene.

Grain-size end member

The end-member modelling analysis algorithm (EMMA) revealed a four-EM model to explain more than 95% of the total variance for each core (Fig. 5). Every core is characterized by four grain classes: end member EM4 is associated with the very coarse silts to fine sands (30–234 µm), end members EM2 and EM3 correspond to the fine to medium (6–18 µm) and medium to coarse (9–63 µm) silts, respectively, and end member EM1 is associated with the clays (<2 µm). The relative contributions of the four end members are plotted against age in Fig. 5. All samples from the three sediment cores are mainly composed of fine-grained detrital sediments (<20 µm). Indeed, the end members EM1+EM2 represented 67, 74 and 78% of the overall grain-size variance for the cores COR0503-CL04-36PC, COR0503-CL05-37PC and COR0602-36PC, respectively. Based on these results, the log(EM2/EM1) ratio is used here to elucidate down-core grain-size variations (silts vs. clay) within the Laurentian Channel detrital sediments, and to investigate sediment transfer and transport conditions during the glaciomarine and postglacial sedimentation.

Mineralogical and geochemical associations

Stratigraphic distributions of the bulk mineralogical and geochemical data from the three sedimentary cores studied here are available electronically in Fig. S2. To gain a better understanding of the mineral and elemental associations and their relationship with sediment samples, PCA was conducted on all sediment cores (Fig. 3). We illustrate the scores from the first two principal components of the log-centred data as these accounts for more than 90% of the total variance. According to PCA results, glaciomarine sediments in the lower St. Lawrence Estuary (COR0602-36PC) are associated mainly with phyllosilicates, K-feldspar and Mg-Cr-Fe-Zn-Al-K-V-LOI, whereas postglacial sediments are characterized by the association of plagioclase-quartz and Si-Zr-Ti-Ca-Sr. In contrast, glaciomarine sediments in the Gulf of St. Lawrence (COR0503-CL04-36PC and COR0503-CL05-37PC) are typified mainly by the association of K-feldspar and plagioclase with Mg-Sr-Cr-K-Al-Fe and to a lesser extent with Si-Ti and Mn, whereas postglacial sediments are associated with phyllosilicates-quartz and Ca-LOI-V-Zn-Mn-Si-Ti-Zr. Similarly, we note that the fine-grained glaciomarine sediments in the estuary are characterized by abundant phyllosilicates, while sediments in the gulf are dominated by K-feldspar and plagioclase (Fig. 3). This most likely suggests that the fine-grained glaciomarine sediments in the gulf contain higher proportions of rock flour derived from glacial erosion of the crystalline rocks on the Canadian Shield (Loring & Nota 1973).

These mineralogical and geochemical differences between the Estuary and Gulf of St. Lawrence may be related to different sediment sources and hydrodynamic sorting. Therefore, based on PCA results, we selected the phyllosilicates/(plagioclase+K-feldspar), log(Zn/Sr), log(Si/K) and Log(Zr/Al) ratios to reconstruct down-core changes in sediment provenance and transport in

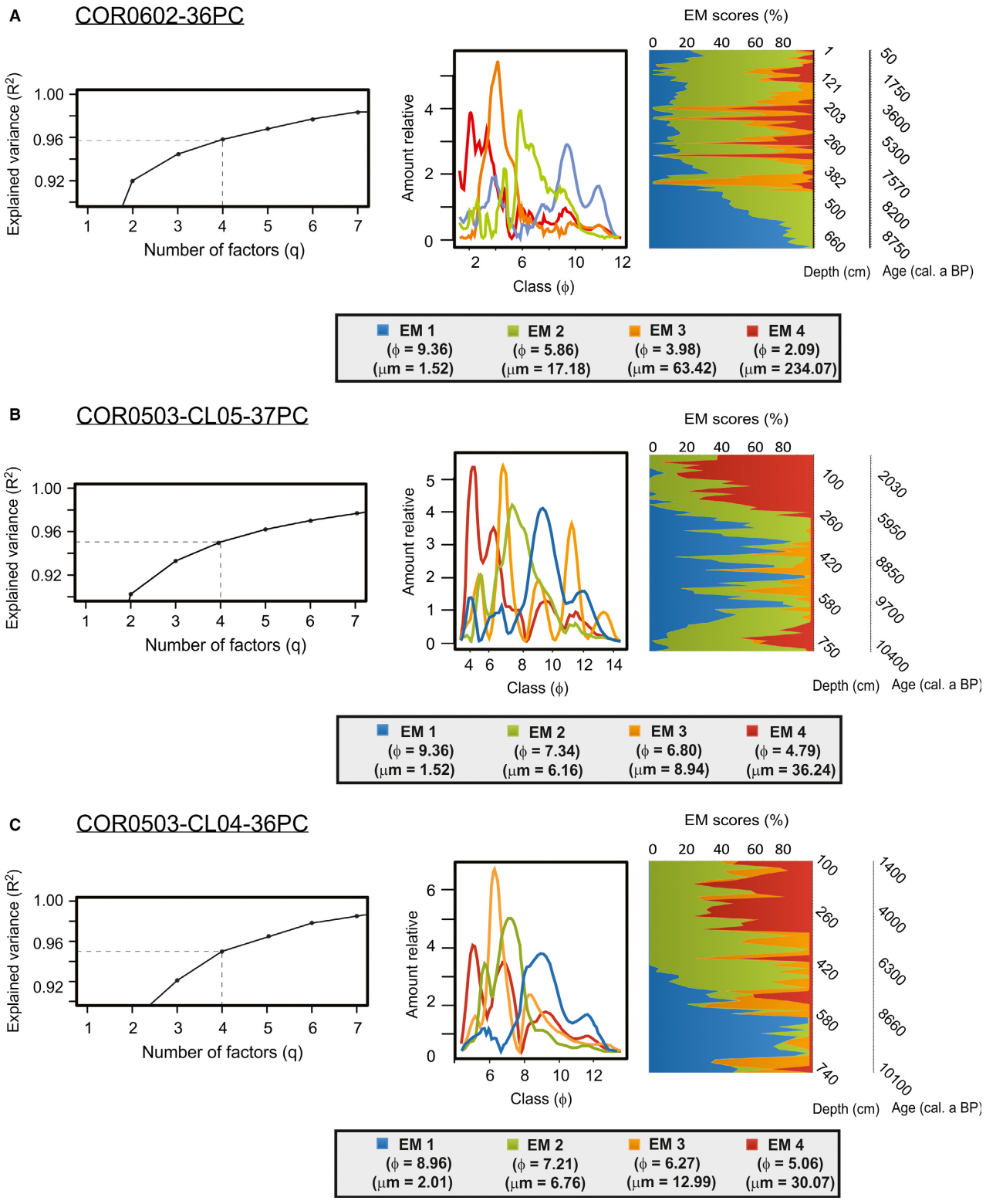

Fig. 5. End-member modelling analyses (EMMA) performed on the grain-size distribution of the detrital fraction of cores COR0602-36PC (A), COR0503-CL05-37PC (B) and COR0503-CL04-36PC (C). The grain-size distribution of the four first end members accounts for more than 95% of the total variance. Four representative unmixed grain-size distributions as well as end-member scores (%) derived from EMMA are shown.

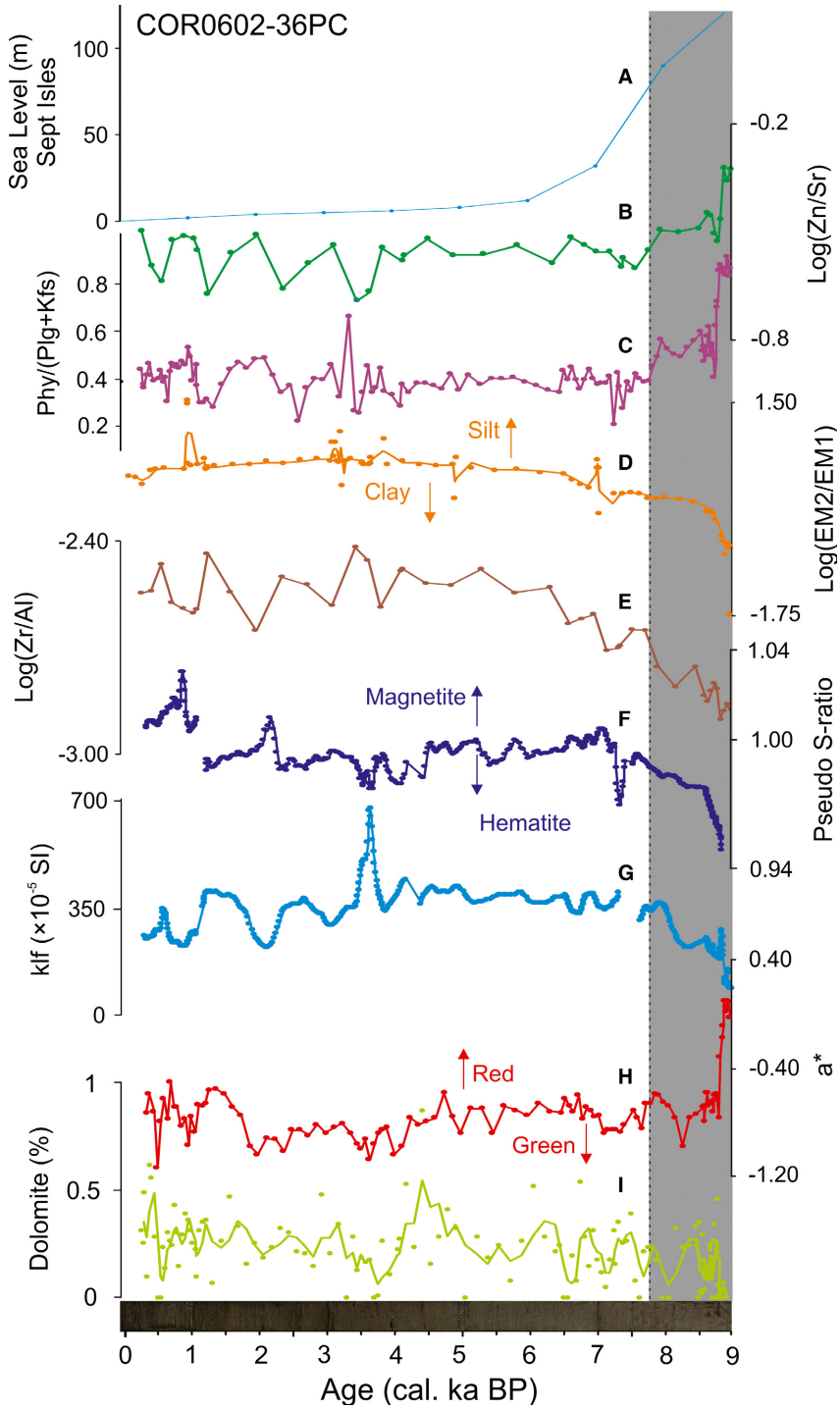

Fig. 6. Multiproxy analysis for core COR0602-36PC. A. Relative sea-level variations at Sept-îles (Shaw *et al.* 2002). B. Geochemical log-ratio Zn/Sr. C. Mineralogical ratio phyllosilicates/(plagioclase+K-feldspar). D. Grain-size end members log(EM2/EM1). E. Geochemical log-ratio Zr/Al. F. Pseudo S-ratio magnetic parameter. G. Magnetic susceptibility (k_{lf}). H. a* indicates sediment colour variations from green to red. I. Dolomite content variations. Note that organic matter and biogenic carbonate were removed with peroxide (30%) and hydrochloric acid (0.5 N), respectively, before bulk mineralogical analysis.

the EGSL over the last 10 cal. ka BP (Figs 6, 7, 8). The phyllosilicates/(plagioclase+K-feldspar) ratio provides a straightforward proxy to discriminate the sediments from the South Shore (Palaeozoic sedimentary rocks) from those from the North Shore (Grenvillian metamorphic rocks). In fact, as suggested in Loring & Nota

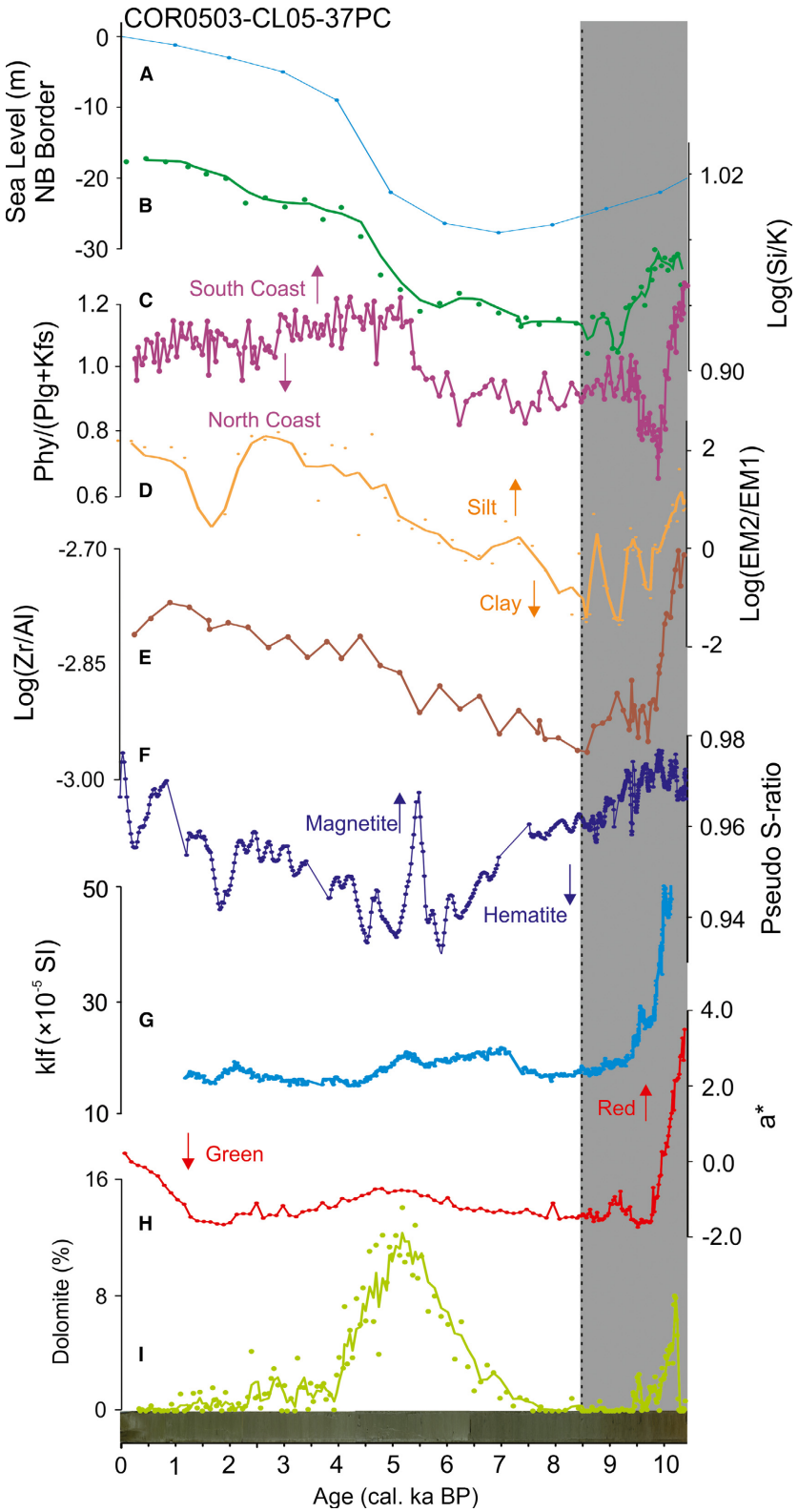

Fig. 7. Multiproxy analysis for core COR0503-CL05-37PC. A. Relative sea level at eastern New Brunswick (Shaw *et al.* 2002). B. Geochemical log-ratio Si/K. C. Mineralogical ratio phyllosilicates/(plagioclase+K-feldspar). D. Grain-size end members log(EM2/EM1). E. Geochemical ratio Zr/Al. F. Pseudo S-ratio magnetic parameter. G. Magnetic susceptibility (k_{lf}). H. a* indicates sediment colour variations from green to red. I. Dolomite content variations. Note that organic matter and biogenic carbonate were removed with peroxide (30%) and hydrochloric acid (0.5 N), respectively, before bulk mineralogical analysis.

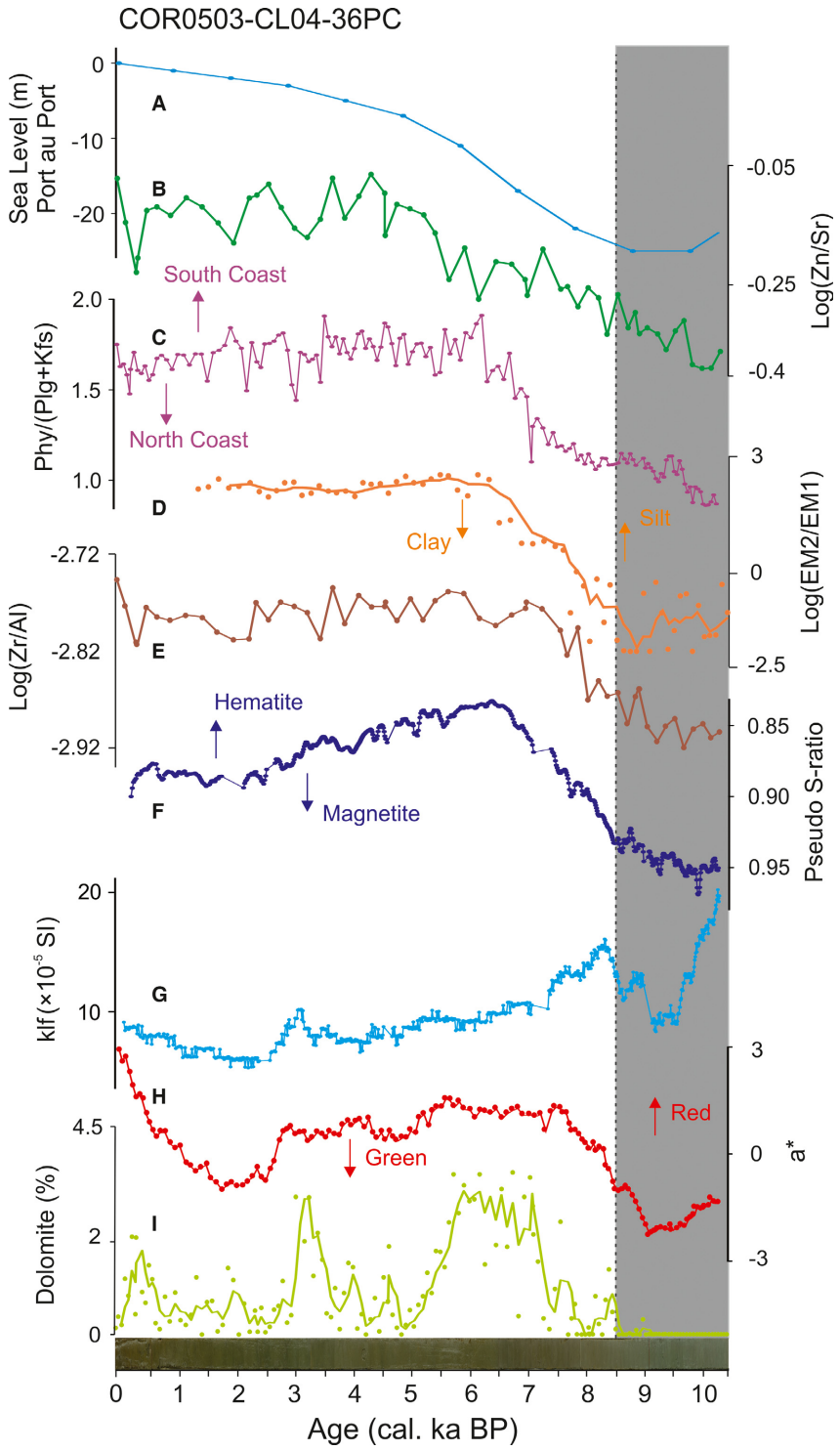

Fig. 8. Multiproxy analysis for sedimentary core COR0503-CL04-36PC. A. Relative sea level at Port au Port (Shaw *et al.* 2002). B. Geochemical log-ratio Zn/Sr. C. Mineralogical ratio phyllosilicates/(plagioclase+K-feldspar). D. Grain-size end members log(EM2/EM1). E. Geochemical log-ratio Zr/Al. F. Pseudo S-ratio magnetic parameter. G. Magnetic susceptibility (k_{lf}). H. a* indicates sediment colour variations from green to red. I. Dolomite content variations. Note that organic matter and biogenic carbonate were removed with peroxide (30%) and hydrochloric acid (0.5 N), respectively, before bulk mineralogical analysis.

(1973) and Jaegle (2015), plagioclases and K-feldspars as well as amphibole, pyroxene and magnetite are more abundant along the North Shore, whereas phyllosilicates, quartz and Fe-oxides (notably, hematite and goethite) are more common along the South Shore and the Canadian Maritime Provinces (on the

southwest gulf). Likewise, the fact that log(Zn/Sr) ratios reflect sediment source is based on preferential Zn concentration in phyllosilicate minerals, whereas Sr is associated with plagioclase-K-feldspar minerals (Fig. 3). However, because Sr may also be associated with Ca in the biogenic and detrital carbonate fraction (notably, dolomite), the presence of high concentrations of carbonates can influence this ratio. In this study, the biogenic carbonates were generally removed from all cores by weak acid treatment; however, dolomite is not always removed following this attack (Figs 6I, 7I, 8I). Such is the case for core COR0503-CL05-37PC, collected close to Anticosti Island, where dolomite contents (Fig. 7I) are particularly high in some intervals (up to 12%) compared to cores COR0602-36PC and COR0503-CL04-36PC (<3%; Figs 6I, 8I). In these circumstances and based on the PCA results, we prefer to use the log(Si/K) ratio rather than log(Zn/Sr) to track changes in sediment provenance south of Anticosti Island (COR0503-CL05-37P). A high log(Si/K) ratio reflects a greater contribution from Si-rich minerals (notably, quartz), whereas low ratios suggest the input of feldspar-rich minerals, notably K-feldspar (Fig. 3). At the same time, changes in sediment grain size were also investigated by comparing the log(Zr/Al) ratios. Zr is concentrated in zircon grains in the coarser fractions, whereas Al is preferentially associated with clay minerals and aluminosilicates in the fine-grained fractions (e.g. Von Eynatten *et al.* 2012).

Laurentian Channel sediment cores

Because the last deglaciation and Holocene sediment dynamics did not evolve synchronously throughout the EGSL (e.g. Dionne 1977; Barletta *et al.* 2010; Levac *et al.* 2015; Rémillard *et al.* 2016), the mineralogical, geochemical, grain-size, magnetic and spectral reflectance results obtained for each sediment core are presented by geographical location as follows:

Lower St. Lawrence Estuary: core COR0602-36PC. – Sediments between 9 and 8 cal. ka BP in core COR0602-36PC are mainly composed of clay (up to 80% EM1) and minor amounts of fine to medium silts (~20% EM2). This grain-size trend is reversed after 8 cal. ka BP with the occurrence of several thin coarser layers (EM3 and EM4; Fig. 5A). The vertical distribution of physical, magnetic, mineralogical and geochemical proxies reveals significant down-core variations (Fig. 6). Indeed, the a* (0.33 to −1.14), log(Zn/Sr) (−0.71 to −0.29) and phyllosilicate/(plagioclase+K-feldspar) (0.95 to 0.22) records show similar patterns, with maximum values in the lowermost part of the core (*c.* 9 cal. ka BP), which sharply decrease between 9 and 8 cal. ka BP, and minimum values with few variations upwards from 8 cal. ka BP to the present. Conversely, the pseudo S-ratio (0.95 to 1.04), magnetic susceptibility (k_{lf}; 67 to 680 × 10^{-5} SI), log(Zr/Al) ratio (−2.92 to −2.42) and log(EM2/EM1) (−0.95 to 1.51) records show minimum values in the lowermost part of the core, which slowly increase between 9 to 8 cal. ka BP, and maximum values with few variations in the uppermost part of the core (8 cal. ka BP to present). Variations in the log(Zr/Al) ratio are well correlated with changes in the proportion of the log(EM2/EM1) ratio (Fig. 6D, E). Detrital carbonate concentrations in this sediment core are negligible (<0.5%) and no major changes are recorded over time.

South of Anticosti Island: core COR0503-CL05-37PC. – In core COR0503-CL05-37PC, the clay (EM1) content increases from 10 to 9 cal. ka BP (up to 96% EM1), remains high but fluctuates between 20–60% until 5 cal. ka BP and then gradually decreases to become almost non-existent from 5 cal. ka BP to the present. The sum of all the coarse fractions (EM2+EM3+EM4) represents more than 80% of the particle size before 9 cal. ka BP, and both the fine to medium silts (EM2) and very coarse silt to fine sand (EM4) particles have dominated over the last 6 cal. ka BP (Fig. 5B). Down-core profiles of pseudo S-ratio, log (EM2/EM1) and log(Zr/Al) ratios show a similar stratigraphic trend, with higher values in the lowermost and uppermost parts of the core (Fig. 7). The magnetic parameter pseudo S-ratio decreases slightly from 0.98 to 0.93 between 10.5–6 cal. ka BP, and then slowly increases up-core (Fig. 7F). The log(EM2/EM1) ratio decreases from 1 to −1 between 10.5–8.5 cal. ka BP, and then slowly increases during the last 8.5 cal. ka BP (Fig. 7D). The log(Zr/Al) ratio shows maximum at the base of the core (up to −2.70) and decreases to reach its minimum at 8.5 cal. ka BP (down to −2.96) and then increases (up to −2.77) up-core (Fig. 7E). Similarly, a* and magnetic susceptibility (k_{lf}) records show maximum values (a* = 3.5; $k_{lf} = 50\times10^{-5}$ SI) in the lowermost parts of the core (10.5–9.5 cal. ka BP), whereas the lowest values (a* = −1.7; $k_{lf} = 14\times10^{-5}$ SI) are characteristically in the uppermost part (Fig. 7G, H). The vertical distribution of phyllosilicates/(plagioclase+K-feldspar) shows maximum at the base of the core (up to 1.27) and decreases to reach its minimum at 9.5 cal. ka BP (down to 0.65) and then increases upwards (up to 1.04) (Fig. 7C). Similar to the mineralogical ratio, the log (Si/K) ratio also reveals higher values (up to 0.97) between 10.5 and 9.5 cal. ka BP, which gradually decreases until 9 cal. ka BP (down to 0.91), and then increases (up to 1.03) during the mid to late Holocene (Fig. 7B). Both phyllosilicates/(plagioclase+K-feldspar) and log(Si/K) depict a sharp upswing centred at about 5 cal. ka BP. High detrital carbonate concentrations (10–12%) are recorded between 10.5–9.5 and 6.5–4 cal. ka BP (Fig. 7I).

Cabot Strait: core COR0503-CL04-36PC. – In core COR0503-CL04-36PC, sediments between 10.5 and 8.5 cal. ka BP are mainly composed of clay (up to 80% EM1), whereas fine to medium silts (EM2) and very coarse silts (EM4) dominate during the last 8.5 cal. ka BP (Fig. 5C). Down-core profiles of phyllosilicates/(plagioclase+K-feldspar) (0.9 to 1.8), log(Zn/Sr) (−0.39 to −0.07) and log(Zr/Al) (−2.95 to −2.75) ratios mimic the stratigraphic trend of the log(EM2/EM1) ratio (−2.12 to 2.40), with the lowest values between 10.5 and 8.5 cal. ka BP, which gradually increase between 8.5 to 6 cal. ka BP, and higher values during the last 6 cal. ka BP (Fig. 8). These detrital proxies show few variations during the last 6 cal. ka BP. The a* record reveals minima in the lowermost (10.5–8.5 cal. ka BP; down to −2.26) and uppermost (2.5–1 cal. ka BP; down to −1.00) parts of the core, and maxima between 8.5–2.5 cal. ka BP (up to 1.52) and during the last 1 cal. ka BP (up to 1.64) (Fig. 8H). The magnetic susceptibility (k_{lf}) record presents maximum (up to 20×10^{-5} SI) in the lowermost parts of the core (10.5–9 cal. ka BP), which decreases abruptly at about 9 cal. ka BP (down to 8.4×10^{-5} SI) and peaks again until *c.* 8 cal. ka BP (up to 16×10^{-5} SI), then slowly decreases (Fig. 8G). The pseudo S-ratio decreases from 0.97 to 0.83 between 10–6 cal. ka BP, and then slowly increase up-core (Fig. 8F). The pseudo S-ratio inversely mimics the stratigraphic trend of the log(EM2/EM1) ratio. Relatively higher detrital carbonate concentrations (up to 3%) are observed between 7–5, 3.5–2.5 and in the last 1 cal. ka BP (Fig. 8I).

Interpretation and discussion

During the last deglaciation, the earth's orbital configuration induced a strong summer insolation maximum and winter insolation minimum in the Northern Hemisphere (Berger & Loutre 1991). This strong boreal summer insolation induced a rapid retreat of the LIS (e.g. Carlson *et al.* 2008, 2009; Montero-Serrano *et al.* 2009, 2011). During this early stage, the rapid hinterland retreat of the LIS triggered major changes in the EGSL system, engendering alterations in proglacial drainage and relative sea level (Fig. 9; Dyke & Prest 1987; Shaw *et al.* 2006).

In this context, the lowermost and the uppermost sedimentary units observed in our three sedimentary cores (Fig. 4) have been interpreted as glaciomarine and postglacial sediments, respectively (Josenhans & Lehman 1999; St-Onge *et al.* 2003). The abrupt change in the mean sedimentation rates from ~300 to ~40 cm ka^{-1} observed in cores COR0602-36PC and COR0503-CL05-37PC around 8.5 cal. ka BP (Fig. 2) was also observed by St-Onge *et al.* (2003) and St-Onge & Long (2009) in cores MD99-2220 and MD99-2221 collected in the lower St. Lawrence Estuary. They associated this observation with a significant reduction in sediment inputs following the re-routing of the LIS meltwaters from the St. Lawrence Estuary to the Hudson Bay and Strait following the catastrophic drainage of the glacial Lake Agassiz-Ojibway at *c.* 8.47 cal. ka BP (Lajeunesse & St-Onge 2008). However, as previously pointed out by Barletta *et al.* (2010), a drastic change in sedimentation rates throughout the Holocene is not observed in the core located at the most seaward location (COR0503-CL04-36PC), possibly because of the scarcity of dated material prior to 8.5 cal. ka BP.

The long-term variations observed in our physical, grain-size, mineralogical, geochemical and magnetic records are discussed below in this context in terms of changes in detrital sediment supply, provenance and transport, and their possible relations with both the deglacial/Holocene climate variability and glacio-isostatic relative sea-level variations.

Sedimentary regime during deglaciation (10–8.5 ka) – meltwater discharges

The high sedimentation rates (~300 cm ka^{-1}) in the thick fine-grained sedimentary successions during deglaciation (10–8.5 cal. ka BP) suggest sedimentary dynamics mainly controlled by the meltwater discharge from the local retreat of the southeastern margin of the LIS on the Canadian Shield (e.g. Syvitski & Praeg 1989; St-Onge *et al.* 2003, 2008). This observation is in agreement with the regional deglaciation pattern of the LIS on the Canadian Shield summarized by Shaw *et al.* (2006). Indeed, around 13 cal. ka BP, large marine areas of Atlantic Canada were ice free (e.g. Rémillard *et al.* 2016), but glaciers remained on most land areas. At 9 cal. ka BP, glacier ice remained only in the Quebec and Labrador regions (Fig. 10). Extensive emerged areas could be found on the Grand Banks and on the Scotian Shelf, and large parts of the southern Gulf of St. Lawrence (Shaw *et al.* 2006). Taken together, these observations highlight the presence of the LIS on the North Shore in the early Holocene (Dyke & Prest 1987; Syvitski & Praeg 1989; Shaw *et al.* 2006), which may explain the large amount of meltwater discharges into the EGSL.

In the lower estuary, the phyllosilicates/(plagioclase+K-feldspar) and Zn/Sr ratios as well as the a* and pseudo S-ratio indicate a mixed provenance of detrital particles between 9 and 8.5 cal. ka BP, that is, mainly from the North Shore, but with a noticeable contribution from the South Shore (Fig. 10). We hypothesize that this sediment mixture is probably due to the close proximity of the LIS margin to the North Shore (e.g. Clark *et al.* 1978; Dyke & Peltier 2000; Shaw *et al.* 2002). The glacio-isostatic loading by the LIS over the lower estuary was greater compared to the Gulf, and induced a higher relative sea level (>100 m) during the early Holocene than at present (Fig. 9A; Clark *et al.* 1978; Shaw *et al.* 2006). Such

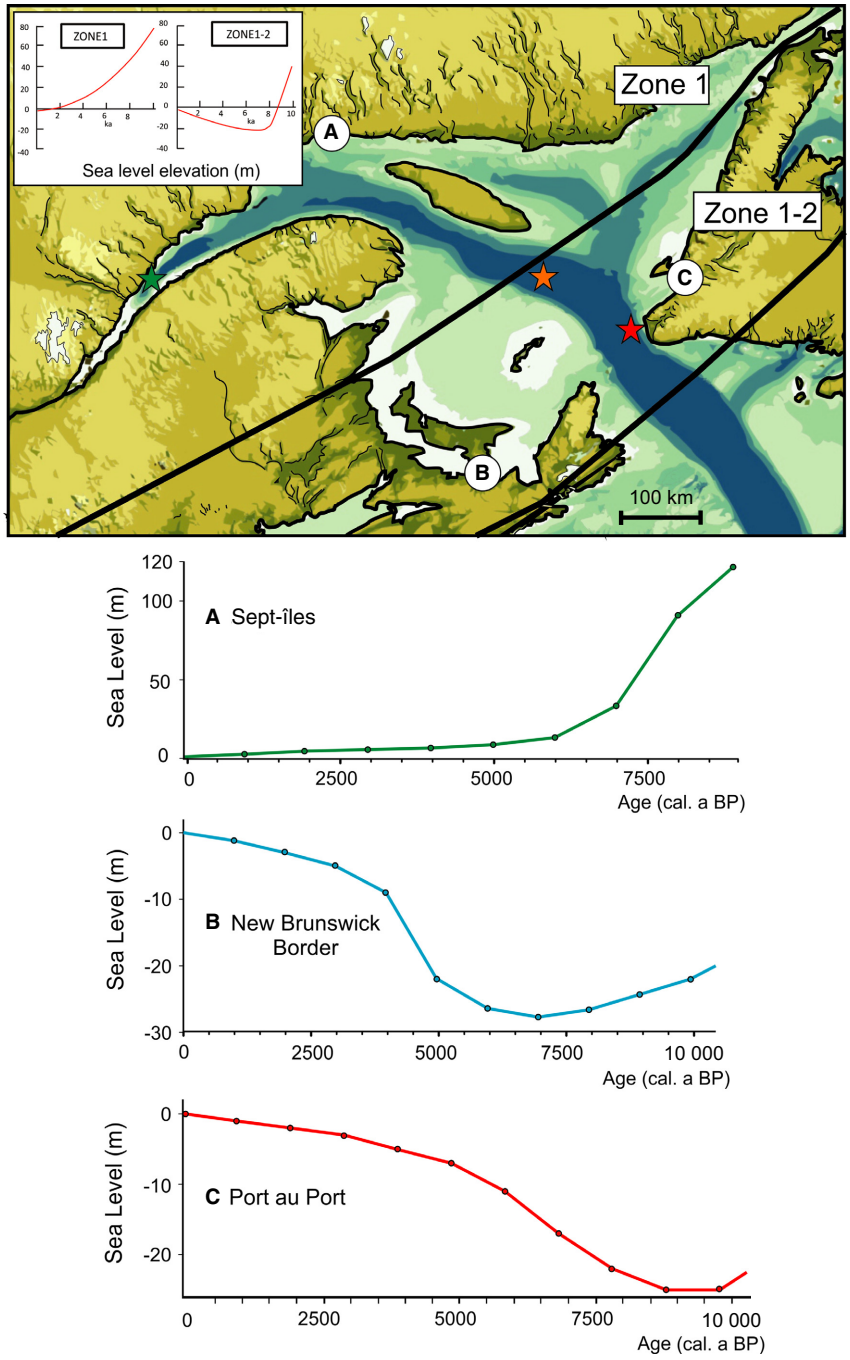

Fig. 9. Evolution of the relative sea level over the last 10 000 years (Shaw *et al.* 2002) represented on three different localities within the Estuary and Gulf of St. Lawrence: Sept-iles (A), New Brunswick border (B) and Port au Port (C). Two zones described by Clark *et al.* (1978) have also been represented (the inset at the top left): Zone 1 had a relative sea level around 80 m higher at 10 cal. ka BP and progressively decreased until today; and Zone 1–2 (a transition zone) had a higher sea level followed by a lower relative sea level around 8 cal. ka BP, and a gradual re-increase in sea level after that. The positions of the three sedimentary cores studied here are also shown.

conditions probably promoted an increase in coastal erosion on the South Shore and, therefore, a larger sediment supply from this area.

In the area south of Anticosti Island (COR0503-CL05-37PC), mineralogical, geochemical and magnetic variations observed between 10.5 and 9.5 cal. ka BP also suggest a mixture of sediment provenances. However, the relative sea level was lower in the Gulf (about −20 to −30 m below present sea level; Shaw *et al.* 2002; Rémillard *et al.* 2016) than in the lower part of the estuary as the LIS margin was more distant (~400 km NW; Shaw *et al.* 2006; Fig. 9). In agreement

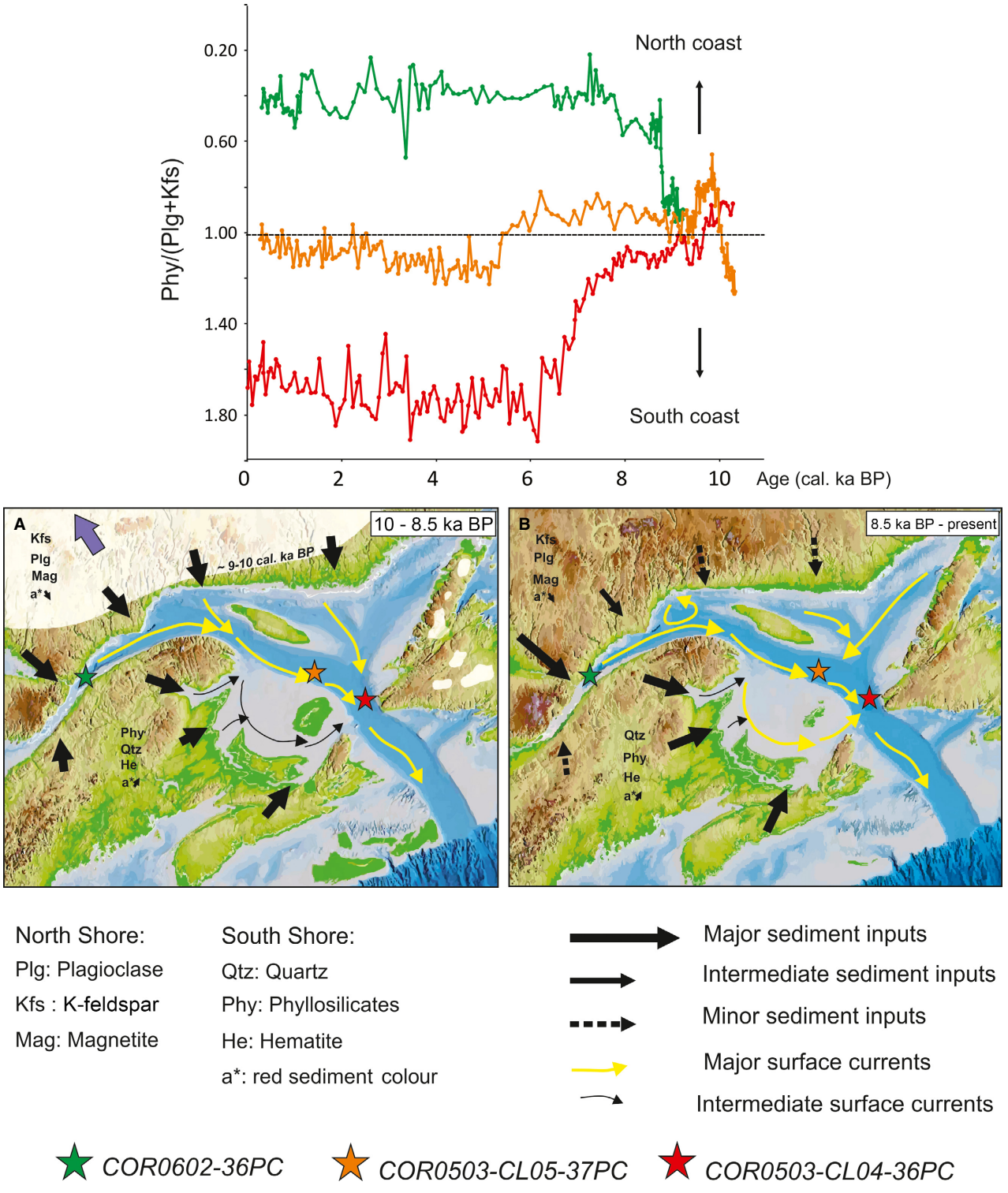

Fig. 10. Evolution of sedimentary dynamics between 10–8.5 cal. ka BP and since 8.5 cal. ka BP. During the early Holocene (A), the sediment dynamics are mainly controlled by the meltwater discharges due to the rapid retreat of the southeastern margin of the LIS on the North Shore (LIS position is schematic for the period from 10 to 9 cal. ka BP; Shaw *et al.* 2002). The sedimentary contribution of the Appalachians is induced by a high relative sea level in the estuary and by a low relative sea level in the gulf, causing a strong erosion of the Magdalen Shelf (modified from Shaw *et al.* 2002). From 8.5 cal. ka BP to the present (B), variations in relative sea level represent the predominant forces acting on the EGSL sediment dynamics. A sharp discrimination of sedimentary sources appears, with the North Shore becoming the main sediment supply in the estuary whereas the South Shore appears as the main sedimentary sources in the gulf.

with Loring & Nota (1973), we hypothesize that these lowstand conditions promoted the remobilization of reddish-brown glacigenic sediments stored on the Magdalen Shelf as well as subsequent transport towards the Laurentian Channel. Surface sediments in the Magdalen Shelf are mainly composed of erosional products derived from Palaeozoic sedimentary rocks of the Appalachian province, which are rich in quartz, phyllosilicates and hematite (which imparts a reddish hue to sediments) and minor amounts of glacigenic sediments derived from crystalline rocks of the Canadian Shield characterized by an abundance of feldspars, amphibole and magnetite (Loring & Nota 1973). The glacigenic materials from the Canadian Shield were transported to the Magdalen Shelf by southward advances of the LIS during the late Wisconsin glaciation (Loring & Nota 1973). Very large increases in a* values (red), the Zr/Al ratio and magnetic susceptibility (k_{lf}) observed at the base of core COR0503-CL05-37PC support the interpretation of the South Shore sedimentary origin (Fig. 7).

Concurrently, in Cabot Strait (COR0503-CL04-36PC), the low phyllosilicates/(plagioclase+K-feldspar) and Zn/Sr ratios as well as higher pseudo S-ratio (magnetite) and magnetic susceptibility (k_{lf}) values observed during the early Holocene suggest that the detrital sediments mainly originated from the North Shore with a minor influence from the Canadian Maritime Provinces. These results are coherent with those obtained by Stevenson *et al.* (2008), whose less-radiogenic εNd signatures obtained on a core taken from the upper slope of the western Grand Banks reveal an increase in the relative contribution of the North American Shield since 13 cal. ka BP.

Furthermore, results obtained from the end-member modelling analysis (EMMA) reveal the dominance of clay and very fine detrital silt particles in the early Holocene in all sediment cores (Fig. 5). This observation is also confirmed by the low Zr/Al ratio values, indicating high amounts of fine-grained Al-rich mineral at the base of all cores. In agreement with several sedimentological studies (e.g. Loring & Nota 1964; Josenhans & Lehman 1999; St-Onge *et al.* 2008, 2011), we hypothesize that sediment-laden meltwater plumes derived from the North Shore, together with a relatively higher sea level than today (Clark *et al.* 1978), induced the accumulation of fine-grained sediments in the ice-distal zones of the EGSL during deglaciation. Indeed, the weak hydrodynamic conditions prevailing in these ice-distal glaciomarine environments caused a less turbulent depositional setting and, therefore, the preferential accumulation of fine-grained sediments.

To summarize, our results suggest that, between 10 to 8.5 cal. ka BP, sediment supply in the EGSL became primarily controlled by the LIS meltwaters from the North Shore and secondarily by glacio-isostatic relative sea-level variations.

Sedimentary regime during the Holocene (8.5 cal. ka BP to present) – postglacial relative sea-level variations

The decrease in the sedimentation rates from about 300 to 40 cm ka^{-1} observed at *c.* 8.5 cal. ka BP (Fig. 2) provides evidence for a drastic decrease in erosional processes in the EGSL as the LIS margin withdrew from its southeasternmost extent and the meltwater discharges re-routed towards Hudson Bay and Strait (St-Onge *et al.* 2003, 2011). Consequently, the variations in grain size, mineralogical, geochemical and magnetic susceptibility observed after 8.5 cal. ka BP cannot be related to changes in the extent of the LIS. Instead, variations in our detrital proxies are most likely related to relative changes in sea level in response to glacio-isostatic rebound (Dionne 1977; Clark *et al.* 1978; Shaw *et al.* 2002, 2006). According to Clark *et al.* (1978), the timing and magnitude of this postglacial isostatic rebound, and therefore changes in relative sea level, were not uniform in eastern Canada. The glacio-isostatic rebound varies spatially depending on both ice thickness and the location of a particular area relative to the ice margin (Licciardi *et al.* 1999; Dyke & Peltier 2000; Dionne & Pfalzgraf 2001; Shaw *et al.* 2002; Rémillard *et al.* 2016). Accordingly, relative sea-level variations were not similar along the east–west coring transect during the last 10 cal. ka BP (Fig. 9). Indeed, one of the cores (COR0602-36PC) was sampled in Zone 1 of Clark *et al.* (1978), which experienced a sea level about 120 m higher at 10 cal. ka BP than the current level, and which has been progressively decreasing to the present. The two other cores (COR0503-CL05-37PC and COR0503-CL04-36PC) were collected in the transition zone (between Zone 1–2), which experienced higher sea level than the present between 10–8 cal. ka BP, then a lower relative sea level around 8 cal. ka BP (around −20 m), and finally, a progressive sea level rise to the present (Fig. 9).

In this context, we compare our detrital proxy data with the relative sea level curve that is closest geographically (Fig. 9) in order to deduce potential relations between relative sea-level variations and sediment dynamics in the EGSL over the last 8.5 cal. ka BP (Figs 6–8). Based on the regional studies of Clark *et al.* (1978) and Shaw *et al.* (2002), we selected three relative sea-level curves along the east–west coring transect: (i) the Sept-îles curve on the North Shore was compared with core COR0602-36PC from the estuary (Fig. 6A), (ii) the eastern New Brunswick curve was compared with core COR0503-CL05-37PC (Fig. 7A), and (iii) the Port au Port curve on Newfoundland's west coast was compared to core COR0503-CL04-36PC (Fig. 8A). All relative sea-level curves reveal a parallel temporal evolution with grain-size, magnetic, mineralogical and geochemical proxies (Figs 6–8). These observations suggest that glacio-isostatic relative sea-level variations have exerted a

significant control on sedimentation in the EGSL over the last 8.5 cal. ka BP.

In the gulf, the mineralogical and geochemical signatures of cores COR0503-CL05-37PC and COR0503-CL04-36PC indicate that detrital sediments derived primarily from the Canadian Maritime Provinces and the South Shore, as evidenced by an increase in phyllosilicates (up to 46%) and quartz (up to 28%) relative to feldspars. Based on coastal currents patterns in the EGSL (Fig. 1A), we suggest that the Appalachian sediments observed in these cores are mainly transported via the Gaspé Current. This current has sufficient energy (21 to 42 cm s^{-1}; Trites 1972; Couillard 1980) to transport Appalachian sediments from the South Shore and Canadian Maritime Provinces to the Gulf (Loring & Nota 1973; Dufour & Ouellet 2007). Indeed, the outward transport that integrates all currents heading toward the ocean near Honguedo Strait ranges between 0.937±0.233 Sv in December and 0.460±0.086 Sv in June (Galbraith *et al.* 2016). According to Sheng (2001), this coastal current is separated into two branches past the tip of the Gaspé Peninsula: the south branch flows over the Magdalen Shelf and along the Canadian Maritime Provinces coast, whereas the north branch flows along the western edge of the Laurentian Channel. In this context, the south branch forms the main outflow of the Gulf on the western side of Cabot Strait and may therefore supply sediments from the Canadian Maritime Provinces to the area from where core COR0503-CL04-36PC was taken. Conversely, the north branch may provide a mix of sediments to the core COR0503-CL05-37PC, with a majority of them mainly originated from the South Shore, and in lower proportion sediments derived from the North Shore.

However, we do not rule out that erosion of the Palaeozoic sedimentary rocks cropping out along the west coast of Newfoundland might also act as a secondary sediment supply to the southern gulf. In fact, the southwestern Newfoundland coast is also characterized by calcareous brownish-red sandstones, as well as reddish and grey limestone and dolostone (Loring & Nota 1973) and, therefore, may also supply phyllosilicates, quartz, dolomite and hematite to the overall sedimentation. The significant increase in a* values (red) and decrease in the pseudo S-ratio (hematite) observed between 8.5 and 2.5 cal. ka BP in core COR0503-CL04-36PC support this observation. Therefore, the detrital carbonate-rich intervals (up to 3%) observed in core COR0503-CL04-36PC (Fig. 8I) at 7–5, 3.5–2.5 and the last 1 cal. ka BP were most likely derived from carbonate outcrops around the southwestern Newfoundland coast. In contrast, we suggest that the carbonate-rich interval (up to 12%) observed in core COR0503-CL05-37PC (Fig. 7I) between 6.5 and 4 cal. ka BP was most likely derived from the coastal erosion of the limestone outcrop on the Anticosti Shelf as relative sea level rose. Overall, our detrital proxies suggest that the progressive and rapid relative sea-level rise in the gulf since 8.5 cal. ka BP promoted shifts in the positions of the shorelines and increases in coastal erosion in the Canadian Maritime Provinces, western Newfoundland and Anticosti Shelf and, therefore, a larger sediment supply from these areas.

In the lower estuary (COR0602-36PC), the low phyllosilicates/(plagioclase+K-feldspar), Zn/Sr and a* values as well as pseudo S-ratio values close to 1 (magnetite) indicate a detrital sediment provenance mainly derived from the North Shore, with the South Shore contributing weakly to overall sedimentation (Fig. 6). These detrital proxies show few noticeable variations over the last 7.5 cal. ka BP, indicating relatively stable sedimentation dynamics through the middle to late Holocene. These results are in agreement with mineralogical interpretations by Jaegle (2015) in surface marine sediments from the St. Lawrence Estuary suggesting that the North Shore is the main source of sediment supply in the estuary. Finally, the concomitant dominance of coarser particles (EM2 to EM4) in the last 7.5 cal. ka BP in all sediment cores suggests that the onset of modern estuarine conditions in the EGSL occurred during the mid-Holocene.

Conclusions

The multiproxy approach performed on three sedimentary cores recovered along an west–east transect in the Laurentian Channel (from its head to its mouth) highlights the evolution and changes of the origin, transport and dynamics of the detrital sediments in the EGSL since the deglaciation. Two sedimentary regimes can be distinguished based on the physical, magnetic, grain-size, mineralogical and geochemical signatures of the sediment cores (Fig. 10):

(i) During deglaciation (10–8.5 cal. ka BP), the high sedimentation rates (~300 cm ka^{-1}), together with specific mineralogical, geochemical and magnetic signatures, suggest that sediment dynamics were mainly controlled by the sediment-laden meltwater discharges from the North Shore resulting from the rapid hinterland retreat of the southeastern margin of the LIS on the Canadian Shield. Moreover, the end-member modelling analysis EMMA and Zr/Al ratio from the three sedimentary cores reveal the dominance of clay and very fine silt detrital particles in the early Holocene, corroborating that sedimentary deposition in the Laurentian Channel took place under an ice-distal glaciomarine environment at that time.

(ii) From 8.5 ka to the present, the retreat of the LIS and the subsequent postglacial movements of the continental crust triggered significant variations in

relative sea level and, therefore, changes in EGSL sedimentary dynamics. Similar trends observed between the relative sea-level curves obtained by Shaw *et al.* (2002) and our mineralogical, geochemical, magnetic and grain-size data suggest that the RSL changes are the predominant forces acting on the EGSL sedimentary dynamics during the last 8.5 cal. ka BP. In the gulf, specific detrital signatures suggest that the South Shore, Canadian Maritime Provinces and western Newfoundland coast are the primary source-area for detrital sediments, with the Canadian Shield province acting as a secondary source. Conversely, detrital supply in the lower estuary remains mainly controlled by the North Shore.

The absence of any major changes in our detrital proxies over the last 7.5 cal. ka BP suggests that the onset of the modern sedimentation regime in the EGSL occurred during the mid-Holocene. Finally, our multiproxy data provide new constraints on the influence of the LIS meltwater discharges and relative sea-level variations on sediment dynamics in the EGSL since the deglaciation.

Acknowledgements. – This research was funded by the FRQ-NT (*établissement de nouveaux chercheurs universitaires* to J.-C. Montero-Serrano) as well as by the Natural Sciences and Engineering Research Council of Canada (NSERC) through Discovery Grants to J.-C. Montero-Serrano and G. St-Onge. We thank the captain, officers, crew and scientific participants of the COR0503 and COR0602 expeditions. These two expeditions were funded through NSERC Ship Time grants to G. St-Onge, P. Lajeunesse and J. Locat. We also acknowledge the financial support of the Canadian Foundation for Innovation (CFI) and Canada Economic Development for Quebec Regions (CED) for the acquisitions of the PANalytical X-ray diffractometer (X'Pert Powder) and X-ray fluorescence (Epsilon 3-XL), respectively. We also thank Quentin Beauvais (ISMER), Joël Chassé (IML) and Marie-Pier St-Onge (ISMER) for their technical support and advice. Finally, we thank Christine Laurin for reviewing the grammar as well as the editor Jan A. Piotrowski and the reviewers Erik S. Rasmussen and Elisabeth Levac for their constructive comments that helped improved the manuscript.

References

Aitchison, J. 1986: *The Statistical Analysis of Compositional Data. Monographs on Statistics and Applied Probability*. 416 pp. Chapman & Hall Ltd., London (reprinted in 2003 by the Blackburn Press, New Jersey).

Aitchison, J. 1990: Relative variation diagrams for describing patterns of compositional variability. *Mathematical Geology 22*, 487–511.

Barletta, F., St-Onge, G., Stoner, J. S., Lajeunesse, P. & Locat, J. 2010: A high-resolution Holocene paleomagnetic secular variation and relative paleointensity stack from eastern Canada. *Earth and Planetary Science Letters 298*, 162–174.

Berger, A. & Loutre, M. F. 1991: Insolation values for the climate of the last 10 million years. *Quaternary Science Reviews 10*, 297–317.

Blaauw, M. & Christen, J. A. 2011: Flexible paleoclimate age-depth models using an autoregressive gamma process. *Bayesian Analysis 6*, 457–474.

Blott, S. J. & Pye, K. 2001: GRADISTAT: a grain size distribution and statistics package for the analysis of unconsolidated sediments. *Earth Surface Processes and Landforms 26*, 1237–1248.

Carlson, A. E., Anslow, F. S., Obbink, E. A., LeGrande, A. N., Ullman, D. J. & Licciardi, J. M. 2009: Surface-melt driven Laurentide Ice Sheet retreat during the early Holocene. *Geophysical Research Letters 36*, L24502, doi: 10.1029/2009GL040948.

Carlson, A. E., Clark, P. U., Haley, B. A., Klinkhammer, G. P., Simmons, K., Brook, E. J. & Meissner, K. J. 2007: Geochemical proxies of North American freshwater routing during the Younger Dryas cold event. *Proceedings of the National Academy of Sciences of the United States of America 104*, 6556–6561.

Carlson, A. E., LeGrande, A. N., Oppo, D. W., Came, R. E., Schmidt, G. A., Anslow, F. S. & Obbink, E. A. 2008: Rapid early Holocene deglaciation of the Laurentide ice sheet. *Nature Geoscience 1*, 620–624.

Clark, J. A., Farrell, W. E. & Peltier, W. R. 1978: Global changes in postglacial sea level: a numerical calculation. *Quaternary Research 9*, 265–287.

COHMAP Members 1988: Climatic changes of the last 18,000 years: observations and model simulations. *Science 241*, 1043–1052.

Couillard, D. 1980: Physico-Chimie des eaux du Golfe et de l'Estuaire Saint-Laurent. *Canadian Water Resources Journal 5*, 55–81.

D'Anglejan, B. F. 1969: Preliminary observations on suspended matter in the Gulf of St. Lawrence. *Maritime Sediment 5*, 15–18.

D'Anglejan, B. F. & Smith, E. C. 1973: Distribution, transport, and composition of suspended matter in the St. Lawrence estuary. *Canadian Journal of Earth Sciences 10*, 1380–1396.

Debret, M., Sebag, D., Desmet, M., Balsam, W., Copard, Y., Mourier, B. & Winiarski, T. 2011: Spectrocolorimetric interpretation of sedimentary dynamics: the new "Q7/4 diagram". *Earth-Science Reviews 109*, 1–19.

Dietze, E., Hartmann, K., Diekmann, B., IJmker, J., Lehmkuhl, F., Opitz, S. & Borchers, A. 2012: An end-member algorithm for deciphering modern detrital processes from lake sediments of Lake Donggi Cona, NE Tibetan Plateau, China. *Sedimentary Geology, 243–244*, 169–180.

Dionne, J.-C. 1977: La mer de Goldthwait au Québec. *Géographie physique et Quaternaire 31*, 61–80.

Dionne, J.-C. 1993: Sediment load of shore ice and ice rafting potential, upper St. Lawrence Estuary, Quebec, Canada. *Journal of Coastal Research 9*, 628–646.

Dionne, J.-C. & Pfalzgraf, F. 2001: Fluctuations holocènes du niveau marin relatif à Rivière-Ouelle, côte sud du moyen estuaire du Saint-Laurent : données complémentaires. *Géographie physique et Quaternaire 55*, 289–300.

Drapeau, G. 1992: Dynamique sédimentaire des littoraux de l'estuaire du Saint-Laurent. *Géographie physique et Quaternaire 46*, 233–242.

Duchesne, M. J. & Bellefleur, G. 2007: Processing of single-channel, high-resolution seismic data collected in the St. Lawrence estuary. *Geological Survey of Canada 2007-D1*, 11 pp.

Duchesne, M. J., Pinet, N., Bédard, K., St-Onge, G., Lajeunesse, P., Campbell, D. C. & Bolduc, A. 2010: Role of the bedrock topography in the Quaternary filling of a giant estuarine basin: the Lower St. Lawrence Estuary, Eastern Canada. *Basin Research 22*, 933–951.

Dufour, R. & Ouellet, P. 2007: Estuary and Gulf of St. Lawrence Marine Ecosystem Overview and Assessment Report. *Canadian Technical Report of Fisheries and Aquatic Sciences*, 112 pp.

Dyke, A. S. & Peltier, W. R. 2000: Forms, response times and variability of relative sea-level curves, glaciated North America. *Geomorphology 32*, 315–333.

Dyke, A. S. & Prest, V. K. 1987: Late Wisconsinan and Holocene History of the Laurentide Ice Sheet. *Géographie physique et Quaternaire 41*, 237–263.

Ebbestad, J. O. R. & Tapanila, L. 2005: Non-predatory borings in Phanerotrema (Gastropoda), Early Silurian, Anticosti Island, Québec, Canada. *Palaeogeography, Palaeoclimatology, Palaeoecology 221*, 325–341.

Galbraith, P. S., Chassé, J., Caverhill, C., Nicot, P., Gilbert, D., Pettigrew, B., Lefaivre, D., Brickman, D., Devine, L. & Lafleur, C. 2016: Physical Oceanographic Conditions in the Gulf of St. Lawrence in 2015. *DFO Canadian Science Advisory Secretariat Research Document 2016/056*, 90 pp.

Grunsky, E. C., Drew, L. J., Woodruff, L. G., Friske, P. W. B. & Sutphin, D. M. 2013: Statistical variability of the geochemistry and mineralogy of soils in the Maritime Provinces of Canada and part of the Northeast United States. *Geochemistry: Exploration, Environment, Analysis 13*, 249–266.

Hargrave, B. T., Bugden, G. L., Head, E. J. H., Petrie, B., Phillips, G. A., Subba Rao, D. V. & Yeats, P. A. 2007: Factors affecting seasonality of lithogenic and biogenic particle flux in a large estuarine ecosystem. *Estuarine, Coastal and Shelf Science 73*, 379–398.

Jaegle, M. 2015: *Nature et origine des sédiments de surface de l'estuaire du Saint-Laurent*. M.Sc. thesis, Université du Québec à Rimouski, 83 pp.

Josenhans, H. & Lehman, S. 1999: Late glacial stratigraphy and history of the Gulf of St. Lawrence, Canada. *Canadian Journal of Earth Sciences 36*, 1327–1345.

King, L. H. & MacLean, B. 1970: Origin of the outer part of the Laurentian Channel. *Canadian Journal of Earth Sciences 7*, 1470–1484.

Koutitonsky, V. G. & Bugden, G. L. 1991: The physical oceanography of the Gulf of St. Lawrence: a review with emphasis on the synoptic variability of the motion. *In* Therrisault, J.-C. (ed.): *The Gulf of St. Lawrence: Small Ocean or Big Estuary*, 57–90. *Canadian Special Publication for Fisheries and Aquatic Sciences 113*.

Lajeunesse, P. & St-Onge, G. 2008: The subglacial origin of the Lake Agassiz-Ojibway final outburst flood. *Nature Geoscience 1*, 184–188.

Levac, E., Lewis, M., Stretch, V., Duchesne, K. & Neulieb, T. 2015: Evidence for meltwater drainage via the St. Lawrence River Valley in marine cores from the Laurentian Channel at the time of the Younger Dryas. *Global and Planetary Change 130*, 47–65.

Licciardi, J. M., Teller, J. T. & Clark, P. U. 1999: Freshwater routing by the Laurentide Ice Sheet during the last deglaciation. *In* Clark, P. U., Webb, S. & Keigwin, D. (eds.): *Geophysical Monograph Series 112*, 177–201. American Geophysical Union, Washington.

Loring, D. H. & Nota, D. J. G. 1964: Recent depositional conditions in the St. Lawrence River and Gulf — A reconnaissance survey. *Marine Geology 2*, 198–235.

Loring, D. H. & Nota, D. J. G. 1973: Morphology and sediments of the Gulf of St. Lawrence. *Bulletin of the Fisheries Research Board of Canada 182*, 147 pp.

Mattheus, C. R., Rodriguez, A. B., Greene, D. L., Simms, A. R. & Anderson, J. B. 2007: Control of upstream variables on incised-valley dimension. *Journal of Sedimentary Research 77*, 213–224.

Montero-Serrano, J.-C., Bout-Roumazeilles, V., Carlson, A. E., Tribovillard, N., Bory, A., Meunier, G., Sionneau, T., Flower, B. P., Martinez, P., Billy, I. & Riboulleau, R. 2011: Contrasting rainfall patterns over North America during the Holocene and Last Interglacial as recorded by sediments of the northern Gulf of Mexico. *Geophysical Research Letters 38*, L14709, doi:10.1029/2011GL048194.

Montero-Serrano, J. C., Bout-Roumazeilles, V., Sionneau, T., Tribovillard, N., Bory, A., Flower, B. P. & Billy, I. 2010a: Changes in precipitation regimes over North America during the Holocene as recorded by mineralogy and geochemistry of Gulf of Mexico sediments. *Global and Planetary Change 74*, 132–143.

Montero-Serrano, J. C., Bout-Roumazeilles, V., Tribovillard, N., Sionneau, T., Riboulleau, A., Bory, A. & Flower, B. 2009: Sedimentary evidence of deglacial megafloods in the northern Gulf of Mexico (Pigmy Basin). *Quaternary Science Reviews 28*, 3333–3347.

Montero-Serrano, J.-C., Föllmi, K. B., Adatte, T., Spangenberg, J. E., Tribovillard, N., Fantasia, A. & Suan, G. 2015: Continental weathering and redox conditions during the early Toarcian Oceanic Anoxic Event in the northwestern Tethys: insight from the Posidonia Shale section in the Swiss Jura Mountains. *Palaeogeography, Palaeoclimatology, Palaeoecology 429*, 83–99.

Montero-Serrano, J. C., Palarea-Albaladejo, J., Martín-Fernández, J. A., Martínez-Santana, M. & Gutiérrez-Martín, J. V. 2010b: Sedimentary chemofacies characterization by means of multivariate analysis. *Sedimentary Geology 228*, 218–228.

Neumeier, U. 2011: Boulder transport by ice on a St. Lawrence saltmarsh, pattern of pluriannual movements. *In* Wang, P., Rosati, J. D. & Roberts, T. M. (eds.): *Coastal Sediments 1*, 2533–2545. World Scientific Publishing, Miami.

Pinet, N., Brake, V., Campbell, C. & Duchesne, M. 2011: Seafloor and shallow subsurface of the St. Lawrence River Estuary. *Geoscience Canada 38*, 31–40.

Piper, D. J. W., Mudie, P. J., Fader, G. B., Josenhans, H. W., MacLean, B. & Vilks, G. 1990: Quaternary geology. *In* Keen, M. J. & Williams, G. L. (eds.): *Geology of the Continental Margin of Eastern Canada*, 475–607. *Geology of Canada, Series 2*. Geological Survey of Canada, Ottawa ON.

Prins, M. & Weltje, G. J. 1999: End-member modeling of siliciclastic grain-size distributions: the late Quaternary record of eolian and fluvial sediment supply to the Arabian Sea and its paleoclimatic significance. *SEPM, Special Publication 62*, 91–111.

Rémillard, A. M., St-Onge, G., Bernatchez, P., Hétu, B., Buylaert, J.-P., Murray, A. S. & Vigneault, B. 2016: Chronology and stratigraphy of the Magdalen Islands archipelago from the last glaciation to the early Holocene: new insights into the glacial and sea-level history of eastern Canada. *Boreas 45*, 604–628.

Saucier, F. J., Roy, F., Gilbert, D., Pellerin, P. & Ritchie, H. 2003: Modeling the formation and circulation processes of water masses and sea ice in the Gulf of St. Lawrence, Canada. *Journal of Geophysical Research 108(C8)*, 3269, doi: 10.1029/2000JC000686.

Scully, M. E. & Friedrichs, C. T. 2007: Sediment pumping by tidal asymmetry in a partially mixed estuary. *Journal of Geophysical Research 112(C7)*, C07028, doi: 10.1029/2006JC003784.

Shaw, J., Gareau, P. & Courtney, R. C. 2002: Palaeogeography of Atlantic Canada 13–0kyr. *Quaternary Science Reviews 21*, 1861–1878.

Shaw, J., Piper, D. J. W., Fader, G. B. J., King, E. L., Todd, B. J., Bell, T. & Liverman, D. G. E. 2006: A conceptual model of the deglaciation of Atlantic Canada. *Quaternary Science Reviews 25*, 2059–2081.

Sheng, J. 2001: Dynamics of a buoyancy-driven coastal jet: the Gaspe Current. *Journal of Physical Oceanography 31*, 3146–3162.

Simon, Q., St-Onge, G. & Hillaire-Marcel, C. 2012: Late Quaternary chronostratigraphic framework of deep Baffin Bay glaciomarine sediments from high-resolution paleomagnetic data: Baffin Bay Late Quaternary stratigraphy. *Geochemistry, Geophysics, Geosystems 13*, Q0AO03, doi: 10.1029/2012GC004272.

Smith, P. C., Petrie, B. D., Elliott, J. A., Oakey, N. S. & Bugden, G. L. 2014: Coastal ocean circulation studies. *In* Nettleship, D. N., Gordon, D. C., Lewis, C. F. M. & Latremouille, M. P. (eds.): *Voyage of Discovery: Fifty Years of Marine Research at Canada's Bedford Institute of Oceanography 17*, 149–157. BIO-Oceans Association, Dartmouth.

Stevenson, R. K., Hollings, P., Meng, X. W. & Hillaire-Marcel, C. 2008: Impact of melting of the Laurentide Ice Sheet on sediments from the upper continental slope off southeastern Canada: evidence from Sm–Nd isotopes. *Canadian Journal of Earth Sciences 45*, 1243–1252.

Stoner, J. S. & St-Onge, G. 2007: Chapter three magnetic stratigraphy in paleoceanography: reversals, excursions, paleointensity, and secular variation. *Developments in Marine Geology 1*, 99–138.

St-Onge, G. & Lajeunesse, P. 2007: Flood-induced turbidites from northern Hudson Bay and western Hudson Strait: a two-pulse record of Lake Agassiz final outburst flood? *In* Lykousis, V., Sakellariou, D. & Locat, J. (eds.): *Submarine Mass Movements and their Consequences*, 129–137. Springer, The Netherlands.

St-Onge, G. & Long, B. F. 2009: CAT-scan analysis of sedimentary sequences: an ultrahigh-resolution paleoclimatic tool. *Engineering Geology 103*, 127–133.

St-Onge, G., Duchesne, M. J. & Lajeunesse, P. 2011: Marine geology of the St. Lawrence Estuary. *IOP Conference Series: Earth and Environmental Science 14*, 012003, doi: 10.1088/1755-1315/14/1/012003.

St-Onge, G., Lajeunesse, P., Duchesne, M. J. & Gagné, H. 2008: Identification and dating of a key Late Pleistocene stratigraphic unit in the St. Lawrence Estuary and Gulf (Eastern Canada). *Quaternary Science Reviews 27*, 2390–2400.

St-Onge, G., Mulder, T., Francus, P. & Long, B. 2007: Continuous physical properties of cored marine sediments. *Developments in Marine Geology 1*, 63–98.

St-Onge, G., Stoner, J. S. & Hillaire-Marcel, C. 2003: Holocene paleomagnetic records from the St. Lawrence Estuary, eastern Canada: centennial- to millennial-scale geomagnetic modulation of cosmogenic isotopes. *Earth and Planetary Science Letters 209*, 113–130.

Stuut, J.-B. W., Temmesfeld, F. & De Deckker, P. 2014: A 550 ka record of aeolian activity near North West Cape, Australia: inferences from grain-size distributions and bulk chemistry of SE Indian Ocean deep-sea sediments. *Quaternary Science Reviews 83*, 83–94.

Syvitski, J. P. M. & Praeg, D. B. 1989: Quaternary sedimentation in the St. Lawrence Estuary and adjoining areas, Eastern Canada: an overview based on high-resolution seismo-stratigraphy. *Géographie physique et Quaternaire 43*, 291–310.

Tang, C. L. & Bennett, A. S. 1981: *Physical Oceanographic Observations in the Northwestern Gulf of St. Lawrence*. 127 pp. Data series BI-D-810–6, Bedford Institute of Oceanography, Dartmouth.

Trites, R. W. 1972: The Gulf of St. Lawrence from a pollution point of view. *In* Ruivo, M. (ed.): *Marine Pollution and Sea Life*, 59–72. FAO Fishing News Books, London.

Van den Boogaart, K. G. & Tolosana-Delgado, R. 2008: "Compositions": a unified R package to analyze compositional data. *Computers and Geosciences 34*, 320–338.

Von Eynatten, H., Barceló-Vidal, C. & Pawlowsky-Glahn, V. 2003: Composition and discrimination of sandstones: a statistical evaluation of different analytical methods. *Journal of Sedimentary Research 73*, 47–57.

Von Eynatten, H., Tolosana-Delgado, R. & Karius, V. 2012: Sediment generation in modern glacial settings: grain-size and source-rock control on sediment composition. *Sedimentary Geology 280*, 80–92.

Von Eynatten, H., Tolosana-Delgado, R., Karius, V., Bachmann, K. & Caracciolo, L. 2016: Sediment generation in humid Mediterranean setting: grain-size and source-rock control on sediment geochemistry and mineralogy (Sila Massif, Calabria). *Sedimentary Geology 336*, 68–80.

Walker, M. J., Berkelhammer, M., Björck, S., Cwynar, L. C., Fisher, D. A., Long, A. J. & Weiss, H. 2012: Formal subdivision of the Holocene Series/Epoch: a Discussion Paper by a Working Group of INTIMATE (Integration of ice-core, marine and terrestrial records) and the Subcommission on Quaternary Stratigraphy (International Commission on Stratigraphy). *Journal of Quaternary Science 27*, 649–659.

Webb, T. III, Anderson, K. H., Bartlein, P. J. & Webb, R. S. 1998: Late Quaternary climate change in Eastern North America: a comparison of pollen-derived estimates with climate model results. *Quaternary Science Reviews 17*, 587–606.

Weltje, G. J. 1997: End-member modeling of compositional data: numerical-statistical algorithms for solving the explicit mixing problem. *Mathematical Geology 29*, 503–549.

Young, R. A. 1993: *The Rietveld Method*. 308 pp. Oxford University Press, New York.

Supporting Information

Additional Supporting Information may be found in the online version of this article at http://www.boreas.dk.

Fig. S1. Comparison of magnetic susceptibility profiles of cores MD99-2221 and COR0602-36PC. Correlative magnetic features are indicated. The last age-depth point of core MD99-2221 was used in the age model of core COR0602-36PC (Fig. 2).

Fig. S2. Vertical distribution of the bulk mineralogical and geochemical data obtained for the sedimentary cores COR0503-CL04-36PC (A, B), COR0503-CL05-37PC (C, D) and COR0602-36PC (E, F).

Table S1. Coordinates and lengths of the three sedimentary piston cores studied herein.